Defense Threat Reduction Agency
8725 John J. Kingman Road, MS
6201 Fort Belvoir, VA 22060-6201

DTRA-TR-17-9

TECHNICAL REPORT

Next Generation Energetic Materials: New Cluster Hydrides and Metastable Alloys of Aluminum in Very Low Oxidation States

October 2016

HDTRA1-12-1-0017

Bryan W. Eichhorn et al.

Prepared by:
Office of Sponsored Programs
University of Maryland
College Park, MD 20742

DESTRUCTION NOTICE:

Destroy this report when it is no longer needed.
Do not return to sender.

PLEASE NOTIFY THE DEFENSE THREAT REDUCTION AGENCY, ATTN: DTRIAC/ J9STT, 8725 JOHN J. KINGMAN ROAD, MS-6201, FT BELVOIR, VA 22060-6201, IF YOUR ADDRESS IS INCORRECT, IF YOU WISH IT DELETED FROM THE DISTRIBUTION LIST, OR IF THE ADDRESSEE IS NO LONGER EMPLOYED BY YOUR ORGANIZATION.

REPORT DOCUMENTATION PAGE

Form Approved
OMB No. 0704-0188

1. REPORT DATE *(DD-MM-YYYY)*	**2. REPORT TYPE**	**3. DATES COVERED** *(From - To)*
00-10-2016	Technical	July 1, 2012 - June 30, 2015

4. TITLE AND SUBTITLE

Next Generation Energetic Materials: New Cluster Hydrides and Metastable Alloys of Aluminum in Very Low Oxidation States

5a. CONTRACT NUMBER
HDTRA-1-12-1-0017

5b. GRANT NUMBER

5c. PROGRAM ELEMENT NUMBER

6. AUTHOR(S)

Bryan W. Eichhorn
Kit H. Bowen
Dennis H. Mayo

5d. PROJECT NUMBER

5e. TASK NUMBER

5f. WORK UNIT NUMBER

7. PERFORMING ORGANIZATION NAME(S) AND ADDRESS(ES)

Office of Sponsored Programs
University of Maryland
College Park, MD 20742

8. PERFORMING ORGANIZATION REPORT NUMBER

9. SPONSORING / MONITORING AGENCY NAME(S) AND ADDRESS(ES)

Defense Threat Reduction Agency
8725 John J. Kingman Road, STOP 6201
Fort Belvoir, VA 22060-6201

10. SPONSOR/MONITOR'S ACRONYM(S)
DTRA

11. SPONSOR/MONITOR'S REPORT NUMBER(S)
DTRA-TR-17-9

12. DISTRIBUTION / AVAILABILITY STATEMENT

Distribution Statement A. Approved for public release; distribution is unlimited.

13. SUPPLEMENTARY NOTES

14. ABSTRACT

We have prepared and fully characterized numerous new Al cluster complexes in low oxidation states by way of wet chemical synthesis, X-ray diffraction experiments, mass spectrometry -- photoelectron spectroscopy experiments, DFT calculations, reactivity studies and other spectroscopic methods. These findings reveal new types of structures and reactivity. To date, 13 papers have been published resulting from full or partial support of this DTRA grant. One additional paper is in under review.

15. SUBJECT TERMS

aluminum clusters, energetic materials, cluster compounds, low oxidation

16. SECURITY CLASSIFICATION OF:			**17. LIMITATION OF ABSTRACT**	**18. NUMBER OF PAGES**	**19a. NAME OF RESPONSIBLE PERSON**
a. REPORT	**b. ABSTRACT**	**c. THIS PAGE**	SAR	38	Allen Dalton
Unclassified	Unclassified	Unclassified			**19b. TELEPHONE NUMBER** *(include area code)* 703-767-3054

UNIT CONVERSION TABLE

U.S. customary units to and from international units of measurement*

U.S. Customary Units	Multiply by → / ← Divide by†		International Units
Length/Area/Volume			
inch (in)	2.54	$\times 10^{-2}$	meter (m)
foot (ft)	3.048	$\times 10^{-1}$	meter (m)
yard (yd)	9.144	$\times 10^{-1}$	meter (m)
mile (mi, international)	1.609 344	$\times 10^{3}$	meter (m)
mile (nmi, nautical, U.S.)	1.852	$\times 10^{3}$	meter (m)
barn (b)	1	$\times 10^{-28}$	square meter (m^2)
gallon (gal, U.S. liquid)	3.785 412	$\times 10^{-3}$	cubic meter (m^3)
cubic foot (ft^3)	2.831 685	$\times 10^{-2}$	cubic meter (m^3)
Mass/Density			
pound (lb)	4.535 924	$\times 10^{-1}$	kilogram (kg)
unified atomic mass unit (amu)	1.660 539	$\times 10^{-27}$	kilogram (kg)
pound-mass per cubic foot (lb ft^{-3})	1.601 846	$\times 10^{1}$	kilogram per cubic meter (kg m^{-3})
pound-force (lbf avoirdupois)	4.448 222		newton (N)
Energy/Work/Power			
electron volt (eV)	1.602 177	$\times 10^{-19}$	joule (J)
erg	1	$\times 10^{-7}$	joule (J)
kiloton (kt) (TNT equivalent)	4.184	$\times 10^{12}$	joule (J)
British thermal unit (Btu) (thermochemical)	1.054 350	$\times 10^{3}$	joule (J)
foot-pound-force (ft lbf)	1.355 818		joule (J)
calorie (cal) (thermochemical)	4.184		joule (J)
Pressure			
atmosphere (atm)	1.013 250	$\times 10^{5}$	pascal (Pa)
pound force per square inch (psi)	6.984 757	$\times 10^{3}$	pascal (Pa)
Temperature			
degree Fahrenheit (^oF)	$[T(^oF) - 32]/1.8$		degree Celsius (^oC)
degree Fahrenheit (^oF)	$[T(^oF) + 459.67]/1.8$		kelvin (K)
Radiation			
curie (Ci) [activity of radionuclides]	3.7	$\times 10^{10}$	per second (s^{-1}) [becquerel (Bq)]
roentgen (R) [air exposure]	2.579 760	$\times 10^{-4}$	coulomb per kilogram (C kg^{-1})
rad [absorbed dose]	1	$\times 10^{-2}$	joule per kilogram (J kg^{-1}) [gray (Gy)]
rem [equivalent and effective dose]	1	$\times 10^{-2}$	joule per kilogram (J kg^{-1}) [sievert (Sv)]

*Specific details regarding the implementation of SI units may be viewed at http://www.bipm.org/en/si/.

†Multiply the U.S. customary unit by the factor to get the international unit. Divide the international unit by the factor to get the U.S. customary unit.

Please answer all sections of the document. You are welcome to use figures and tables to complement or enhance the text. For annual reports, please only describe work for the period of performance (July 1, 2013 - June 30, 2014). For final reports, please describe the comprehensive effort.

Grant/Award #: HDTRA-1-12-1-0017
PI Name: Bryan Eichhorn (PI), Kit Bowen (co-I), Dennis Mayo (co-I)
Organization/Institution: University of Maryland (lead), Johns Hopkins, NSWC-Indian Head
Project Title: ***Synthetic and Mechanistic Reactivity Studies of Low Oxidation State Aluminum Clusters and Particles for Energetic and Agent Defeat Applications***

What are the major goals of the project?
List the major goals of the project as stated in the approved application or as approved by the agency. If the application lists milestones/target dates for important activities or phases of the project, identify these dates and show actual completion dates or the percentage of completion. Generally, the goals will not change from one reporting period to the next. However, if the awarding agency approved changes to the goals during the reporting period, list the revised goals and objectives. Also explain any significant changes in approach or methods from the agency approved application or plan.

The major goals of the project are to **1)** discover and characterize new low-oxidation state Al-Si-H and Al-Zn-H bimetallic hydrides and Al-based clusters with a variety of ligands in the gas phase, **2)** prepare macroscopic quantities of the new, low oxidation state aluminum-containing cluster materials, Al-E bimetallic hydrides (E = Si, B, Zn) and metastable AlM nanoparticle (NP) alloys, where M = Si, Zn by using AlCl and AlBr precursors prepared from our unique metal-halide co-condensation reactor, and **3)** fully characterize the kinetic, thermodynamic, explosive and spectroscopic properties of the cluster compounds.

What was accomplished under these goals?

For this reporting period describe: 1) major activities; 2) specific objectives; 3) significant results, including major findings, developments, or conclusions (both positive and negative); and 4) key outcomes or other achievements. Include a discussion of stated goals not met. As the project progresses, the emphasis in reporting in this section should shift from reporting activities to reporting accomplishments.

We have prepared new cluster compounds with model energetic ligand systems; namely an Al(II) pyrazolate anion $Na_2Al_2(Ph_2pz)_6$, (**1**), where Ph_2pz is 3,5-diphenyl pyrazolate (Fig 1a) and a highly unusual $Li_8Al_2[4\text{-Me-}C_6H_3N(SiMe_3)]_6\bullet 2THF$ complex, (**2**), (Fig. 1b) which also formally has A(II) ions. Complex **1** is the first low valent pyrazolate Al complex and its structure has $Na(Ph_2pz)_3$ units that are strikingly similar to a tris-pyrazolylborate (tpb) ligands (with Na in place of BH). First, this result suggests that series of low oxidation state tpb and pz *anionic* complexes may be accessible if we can accommodate the countercations and, second, that low valent Al complexes are indeed compatible with model energetic ligands (a major goal of HDTRA-1-12-1-007). A report on this compound can be found in Reference Complex **2** has a remarkable Li_8Al_2 core that has the shortest Li-Al interaction known (2.609 Å) and is a true intermetalloid (Fig. 1b). We have also discovered a series of AlM and AlMH intermetallic complexes in molecular beam and photoelectron studies (M = Mg, Au, Sn, Mo, Ni, Zn) that preliminarily show similarities to the solution chemistry (Fig. 1c). These results show that AlM hydrides and intermetalloids are isolable (also a major goal of HDTRA-1-12-1-007) and that "hard" Al-aryl ligands are preferred over Al-amide bonds in solution phase synthesis.

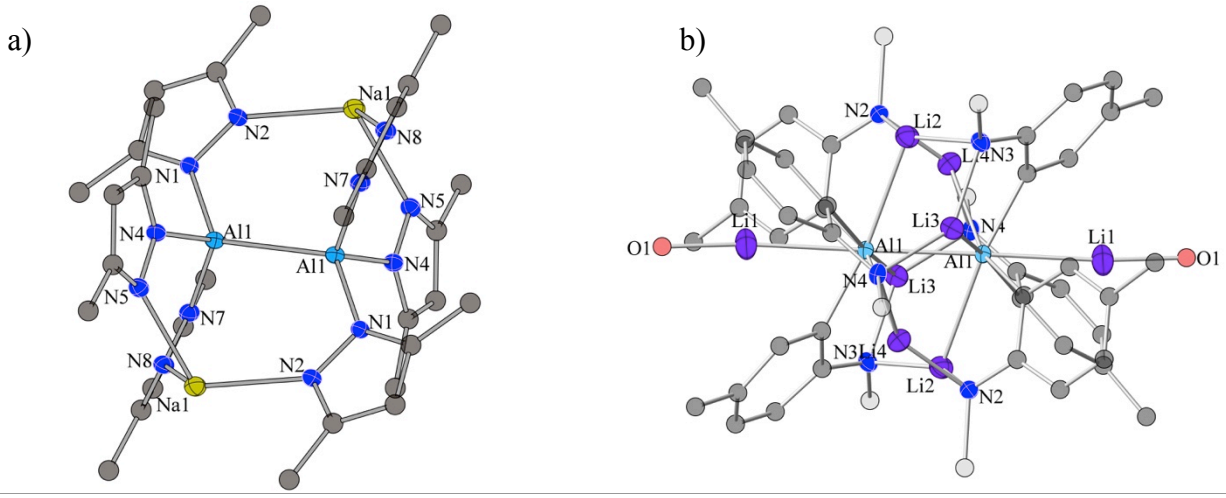

Figure 1: Single crystal x-ray structures of a) $Na_2Al_2(Ph_2pz)_6$, (1), and b) $Li_8Al_2[4\text{-Me-}C_6H_3N(SiMe_3)]_6\bullet 2THF$. Aluminum = light blue, carbon = dark gray, lithium = purple, nitrogen = dark blue, oxygen = red, silicon = light gray, sodium = yellow.

Recently, we also have obtained the first examples of structurally characterized $Al(R\text{-bipy})_3$ complexes (where R = Me or ^{t}Bu, see Figure 2) and have fully characterized their magnetic, electrochemical, and spectroscopic properties. These neutral compounds both contain an Al^{3+} ion and three anionic $[bipy]^{1-}$ ligands and appear to each have seven electrochemically accessible

species in their electrochemical series. The magnetic properties of these two species are remarkably different, with the Al(Me-bipy)$_3$ showing low-temperature antiferromagnetic ordering.

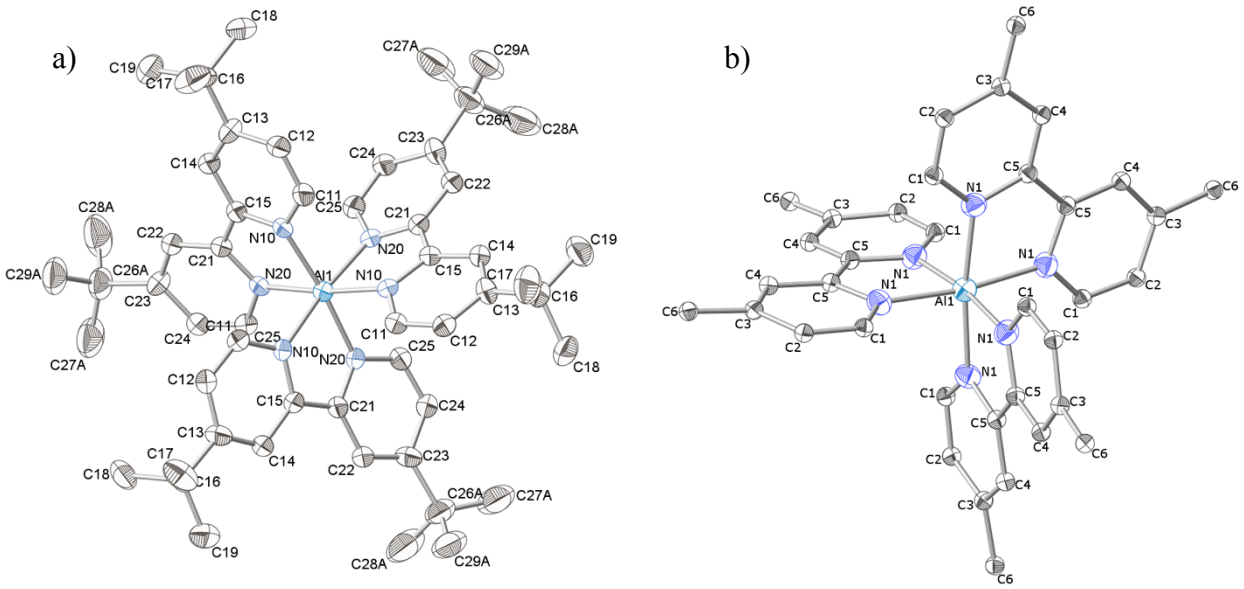

Figure 2: Single-crystal x-ray structures of a) Al(tBu-bpy)3 and b) Al(Me-bpy)3. Aluminum = light blue, carbon = gray, nitrogen = dark blue.

Based on the Al–C bonding present in **2**, reactions between aryl ligands and aluminum monohalides were undertaken, resulting in the formation and characterization of an $[Li_4Al(AlPh_3)_4]^-$ cluster (**3**). Compound **3** contains a central Al^0 atom surrounded by four $[AlPh3]^-$ moieties in a perfect tetrahedral arrangement (see Figure 3). Additionally, a number of forms of $LiAlPh_4$ and $LiGaPh_4$ were isolated and characterized from the same reactions mixtures.

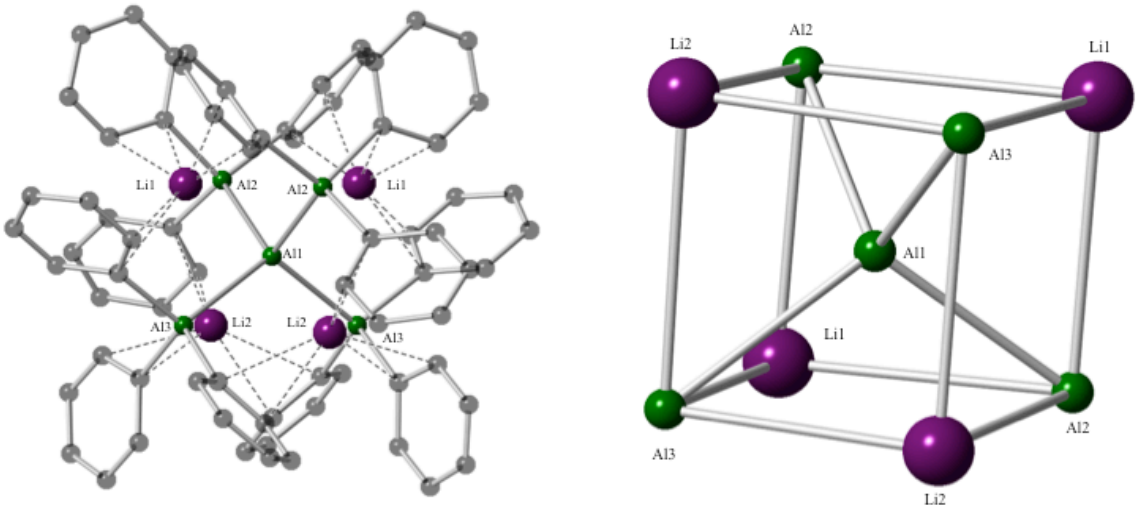

Figure 3: (a) Ball and stick model of 1 (left) and the $[Li_4Al_5]^{11+}$ cluster core (right). Aluminum = green, lithium = violet, carbon = gray. Al-Li interactions are shown only to illustrate the resemblance of the core of structure 1 to a substituted heterocubane.

We have also extracted the structure of a ligated aluminum cluster using the synergetic combination of anion photoelectron spectroscopy and computations, developed a method for capturing small samples of aluminum hydride clusters, built an electrospray source and integrated it into an anion photoelectron spectrometer, synthesized new classes of low oxidation state Al compounds by reacting aluminum hydride clusters with ligands in a reaction cell, and developed a surface cluster reactivity system that allows us to study cluster oxidation chemistry and thermodynamics. Our studies on the oxidation of $Li_2Al_3(PPh_2)_6^{1-}$ showed that initial reactivity occurs at the reduced aluminum core and that ligand fragments are initially expelled in un-oxidized forms. This result has important implications for the use of Al clusters as energetic materials. A major concern of employing ligated Al clusters in energetic applications is that combustion of the outer ligands would consume a significant portion of the ambient oxygen, thereby impeding the combustion of the energetically-rich Al core. The data from the JHU oxidation experiment are in excellent agreement with the theoretical studies of *Hooper* on $Cp^*_{12}Al_{50}$ oxidation, which also suggest that Al combustion *precedes* ligand oxidation and maximizes energy output.

Additional collaboration with NPS (Hooper) has resulted in theoretical studies on aluminum nanoparticle nucleation on functionalized graphene surfactants from aluminum monochloride solutions. This data shows a strong affinity of AlCl units for graphene vacancy sites; adsorption of AlCl to the site results in oxidative insertion into the Al–Cl bond and formation of an Al(III) center. Preliminary studies on the formation of aluminum nanoparticles from AlCl solutions show the formation of Al metal in the presence of $LiAlH_4$. These nanoparticles can be stabilized on a graphene surface, and TEM analysis shows an average nanoparticle size of ~30 nm (see Figure **4**).

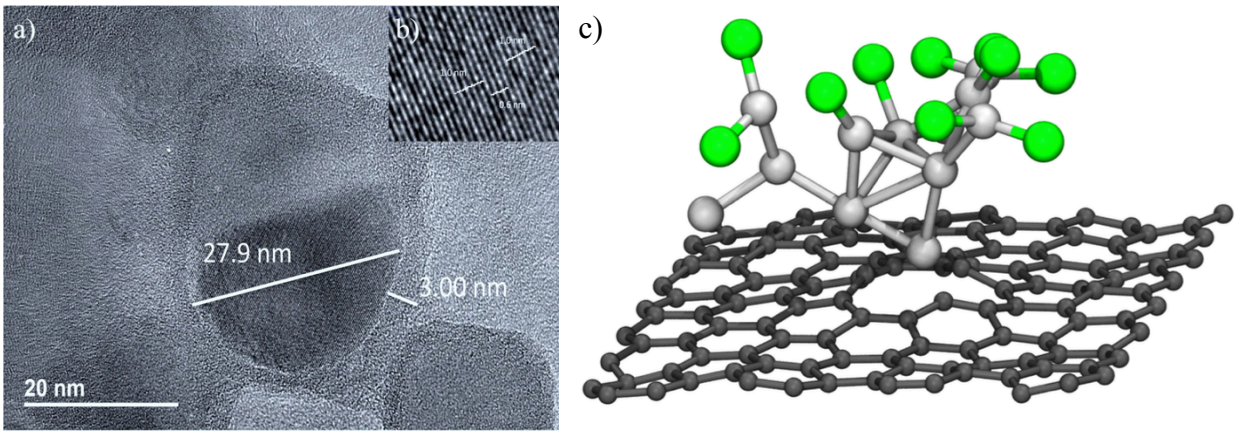

Figure 4: a) HR-TEM image of Al-NPs deposited on graphene surface; b) inset showing Al 100 lattice fringes; c) atomistic simulations of nanoparticle growth from AlCl precursor at graphene defect site (from Reference 1).

What opportunities for training and professional development has the project provided?
If the research is not intended to provide training and professional development opportunities or there is nothing significant to report during this reporting period, state "Nothing to Report." Describe opportunities for training and professional development provided to anyone who worked on the project or anyone who was involved in the activities supported by the project. "Training" activities are those in which individuals with advanced professional skills and experience assist others in attaining greater proficiency. Training activities may include, for example, courses or one-on-one work with a mentor. "Professional development" activities result in increased knowledge or skill in one's area of expertise and may include workshops, conferences, seminars, study groups, and individual study. Include participation in conferences, workshops, and seminars not listed under major activities.

Training: Students and postdocs learn unique skills that involve manipulating air-sensitive and energetic materials in a safe, effective manner. They also learn skills of synthesis, spectroscopy, chemical kinetics, chemical thermodynamics, structural analysis and problem solving. They also learn to work in a team environment.

Professional Development: Students and postdocs have presented their internally and received feedback on their performances. One presentation by graduate student (Samantha DeCarlo) at 2015 ACS conference (Denver, CO). One course taught in Tübingen (Germany) by postdoctoral research assistant (Dr. Christopher Snyder).

How have the results been disseminated to communities of interest?
If there is nothing significant to report during this reporting period, state "Nothing to Report." Describe how the results have been disseminated to communities of interest. Include any outreach activities that have been undertaken to reach members of communities who are not usually aware of these research activities, for the purpose of enhancing public understanding and increasing interest in learning and careers in science, technology, and the humanities.

To date we have published 14 papers to date that resulted from full or partial DTRA support.

1. "Synthesis, Structure and Properties of $Al(^{R}bpy)_3$ Complexes(R = t-Bu, Me): Homoleptic Main-Group tris-bipyridyl Compounds", DeCarlo, S.; Mayo, D. H.; Tomlinson, W.; Hu, J.; Hooper, J.; Zavalij, P; Bowen, K.; Schnöckel, H.; Eichhorn, B. *Inorganic Chemistry,* submitted Jan 2016.

2. "Growth of metalloid aluminum clusters on graphene vacancies", Alnemrat, S.; Mayo, D. H.; DeCarlo, S.; Hooper, J. *J Chem. Phys,* **144**, 024703 (2016)

3. "Synthesis, structure, and properties of a dialumane supported by pyrazolate ligands", Snyder, C. J.; Zavalij, P.; Bowen, K. H.; Schnöckel, H.; Eichhorn, B. W. *Dalton Transactions*. **44**, 2956–2958 (2015)

4. "Photoelectron Spectroscopy of Boron Aluminum Hydride Cluster Anions", H. Wang, X. Zhang, Y. Ko, G. F. Gantefor, K. H. Bowen, X. Li, K. Boggavarapu, and A. Kandalam , *J. Chem. Phys.* **140**, 164317 (2014)

5. "The Viability of Aluminum Zintl Anion Moieties within Magnesium-Aluminum Clusters ", H. Wang, Y. Ko, X. Zhang, G. Gantefoer, H. Schnoeckel, B. W. Eichhorn, P. Jena, B. Kiran, A. K. Kandalam, and K. H. Bowen, *J. Chem. Phys*. **140**, 124309 (2014)

6. " Very Small 'Window of Opportunity' for Generating CO Oxidation-Active Au_n on TiO_2 ", X. Tang, J. Schneider, A. Dollinger, Y. Luo, A. S. Wörz, K. Judai, S. Abbet, Y. D. Kim, G. F. Ganteför, D. H. Fairbrother, U. Heiz, K. H. Bowen and S. Proch, *Phys. Chem. Chem. Phys. ,* **16**, 6735-6742 (2014)

7. "Photoelectron Spectroscopic Study of the Diphenylphosphide Anion and Its Oxide", X. Zhang, X. Tang, D. H. Mayo, S. DeCarlo, B. Eichhorn, K. H. Bowen, *Chem. Phys. Lett. ,* **597**, 110 −113 (2014)

8. "The Reaction Rates of O_2 with Closed-Shell and Open-Shell Al_x^- and Ga_x^- Clusters under Single Collision Conditions: Experimental and Theoretical Investigations towards a generally Valid Model for the Hindered Reactions of O_2 with Metal Atom Clusters", M. Neumaier, M. Olzmann, K. Boggavarapu, K. H. Bowen, B. Eichhorn, S. Stokes, A. Buonaugurio, R. Burgert, H. Schnoeckel, *J. Am. Chem. Soc.,* **136**, 3607–3616 (2014)

9. "Aluminum Zintl Anion Moieties within Sodium Aluminum Clusters", H. Wang, X. Zhang, J. Ko, A. Grubisic, X. Li, G. Ganteför, H. Schnöckel, B. Eichhorn, M. Lee, P. Jena, A. Kandalam, B. Kiran, and K. H. Bowen, *J. Chem. Phys.* **140,** 054301 (2014)

10. "$K[Al_4(PPh_2)_7PPh$: An AlII Phosphanide / Phosphinidene -Intermediate on the Path to AlP Formation ", D. H. Mayo, Y. Peng, S. DeCarlo, X. Li, J. Lightstone, P. Zavalij, K. H. Bowen, H. Schnoeckel, B. Eichhorn, *Zeitschrift fuer Anorganische und Allgemeine Chemie,* **639**, 2558(2013)

11. "Aluminium(III) Amidinates Formed from Reactions of 'AlCl' with Lithium Amidinates ", D. H. Mayo, Y. Peng, P. Zavalij, K. H. Bowen and B. W. Eichhorn, *Acta Cryst.* **C69**, 1120-1123(2013)

12. "Development of Metal Cluster-Based Energetic Materials at NSWC-IHD", J. Lightstone, C. Stoltz, R. M. Wilson, J. M. Horn, J. Hooper, D. Mayo, B. Eichhorn, K. H. Bowen, and M. G. White, *AIP Conf. Proc.* **1426**, 611 (2012)

13. "Tetrabromidobis(dicyclohexylphosphane-κ*P*)digallium(*Ga*-*Ga*)", D. H. Mayo, Y. Peng, P. Zavalij, K. H. Bowen and B. W. Eichhorn, *Acta Cryst.* E**68**, m1245 (2012)

14. "Magnetic Structure Variation in Manganese-Oxide Clusters", K. S. Williams, J. P. Hooper, J. M. Horn, J. M. Lightstone, H. Wang, Y. J. Ko, and K. H. Bowen, *J. Chem. Phys.*, **136**, 134315 (2012)

What do you plan to do during the next reporting period to accomplish the goals?
If there are no changes to the agency-approved application or plan for this effort, state "No Change." Describe briefly what you plan to do during the next reporting period to accomplish the goals and objectives.

We will continue our program with modifications designed to overcome some of the challenges we faced in this chemistry. Specifically, **1**) overcome the crystallization problems that plague Al cluster chemistry in order to elucidate the structures of new Al cluster compounds, **2**) prepare new Al cluster compounds by using ligand types that proved successful in our previous award period and those identified through theoretical targeting, **3**) explore the reactivity of isolated clusters and graphene-stabilized Al particles for use in C-WMD applications.

JACS
JOURNAL OF THE AMERICAN CHEMICAL SOCIETY
Article
pubs.acs.org/JACS

The Reaction Rates of O_2 with Closed-Shell and Open-Shell Al_x^- and Ga_x^- Clusters under Single-Collision Conditions: Experimental and Theoretical Investigations toward a Generally Valid Model for the Hindered Reactions of O_2 with Metal Atom Clusters

Marco Neumaier,[†] Matthias Olzmann,*[,†] Boggavarapu Kiran,[§] Kit H. Bowen,[‡] Bryan Eichhorn,[⊥] Sarah T. Stokes,[‡] Angela Buonaugurio,[‡] Ralf Burgert,[†] and Hansgeorg Schnöckel*[,†]

[†]Institut für Anorganische Chemie and Institut für Physikalische Chemie, Karlsruher Institut für Technologie (KIT) Campus Süd, Postfach 6980, D-76049 Karlsruhe, Germany

[§]Department of Chemistry, McNeese State University, 4205 Ryan Street, Lake Charles, Louisiana 70609, United States

[‡]Department of Chemistry, Johns Hopkins University, 3400 North Charles Street, Baltimore, Maryland 21218, United States

[⊥]Department of Chemistry and Biochemistry, University of Maryland, College Park, Maryland 20742, United States

Supporting Information

ABSTRACT: In order to characterize the oxidation of metallic surfaces, the reactions of O_2 with a number of Al_x^- and, for the first time, Ga_x^- clusters as molecular models have been investigated, and the results are presented here for $x = 9-14$. The rate coefficients were determined with FT-ICR mass spectrometry under single-collision conditions at O_2 pressures of $\sim 10^{-8}$ mbar. In this way, the qualitatively known differences in the reactivities of the even- and odd-numbered clusters toward O_2 could be quantified experimentally. To obtain information about the elementary steps, we additionally performed density functional theory calculations. The results show that for both even- and odd-numbered clusters the formation of the most stable dioxide species, $[M_xO_2]^-$, proceeds via the less stable peroxo species, $[M_x^+\cdots O_2^{2-}]^-$, which contains M−O−O−M moieties. We conclude that the formation of these peroxo intermediates may be a reason for the decreased reactivity of the metal clusters toward O_2. This could be one of the main reasons why O_2 reactions with metal surfaces proceed more slowly than Cl_2 reactions with such surfaces, even though O_2 reactions with both Al metal and Al clusters are more exothermic than are reactions of Cl_2 with them. Furthermore, our results indicate that the spin-forbidden reactions of $^3O_2$ with closed-shell clusters and the spin-allowed reactions with open-shell clusters to give singlet $[M_x^+\cdots O_2^{2-}]^-$ are the root cause for the observed even/odd differences in reactivity.

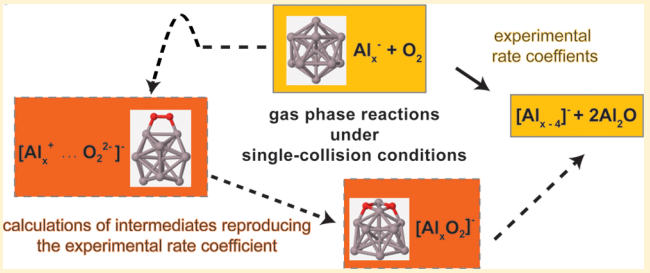

INTRODUCTION

The hindered reactivity of O_2 with metal surfaces, in contrast to their fast reactions with Cl_2, is well-known in classical inorganic chemistry[1] and is based on some important differences between these reactants.

In the case of a base metal such as Al, the O_2 reaction is strongly exothermic with respect to the formation of Al_2O_3 ($2Al + {}^3/_2O_2 \rightarrow Al_2O_3$: $\Delta H_f^\circ = -1676$ kJ mol^{-1}, that is, 838 kJ per 1 mol Al), while less energy is gained in the Cl_2 reaction, where $AlCl_3$ is formed ($Al + {}^3/_2Cl_2 \rightarrow AlCl_3$: $\Delta H_f^\circ = -705$ kJ mol^{-1}).[2] Because of the high stability of Al_2O_3, it remains steadfastly on the surface of the aluminum metal, protecting it and prohibiting further oxidation of the metal. Only at high temperatures >1200 °C, where Al_2O_3 reacts with Al metal to form the low valent oxide molecule Al−O−Al, can alumina be vaporized and removed from the metal surface.[3] The formation of this linear molecule, Al−O−Al, is the essential step in the deterioration of the aluminum surface after reaction of O_2 with solid Al and, as we will see, with Al_x^- clusters:[4]

$$Al_x^- + O_2 \rightarrow Al_{x-4}^- + 2Al_2O_{(g)} \quad (1a)$$

If an excess of O_2 is applied, the Al_2O molecules are easily oxidized to solid Al_2O_3, and simultaneously a large amount of energy is gained:

$$Al_2O_{(g)} + O_{2(g)} \rightarrow Al_2O_{3(s)} \quad (1b)$$

with $\Delta_R H^\circ = -1530.5$ kJ mol^{-1}.[2] In contrast, the chlorination of Al runs at even low temperatures (>200 °C), and the reaction proceeds completely to $AlCl_3$ (or to Al_2Cl_6), which is a volatile solid compound even at these temperatures. Therefore, this reaction continues until the Al metal is consumed.[5,6]

Received: December 10, 2013
Published: February 24, 2014

   dx.doi.org/10.1021/ja4125548 | J. Am. Chem. Soc. 2014, 136, 3607−3616

Besides the thermodynamic data and experimental results, which favor a fast and complete reaction of Al metal with Cl_2 in comparison to O_2, there is a molecular-kinetic reason for the slower reaction of O_2, a stepwise transfer of four electrons from Al to O_2 via several intermediates containing AlO bonds:

$$O_2 \xrightarrow{e^\ominus} O_2^- \xrightarrow{e^\ominus} O_2^{2-} \xrightarrow{2e^\ominus} 2O^{2-}$$

(superoxo) (peroxo) (oxide)

In contrast, in the case of Cl_2 only one intermediate is possible, which contains two AlCl bonds, because every Cl_2 molecule takes two electrons to form two Cl^- anions.

The investigation of the complex reaction of O_2 molecules with metal atom surfaces was and still is a challenging problem for theory and experiment.[7] On the experimental side, it mainly had been dealt with by physicists using surface methods such as atomic force microscopy (AFM) and scanning tunneling microscopy (STM).[7] However, the investigation of surfaces of base metals bears a fundamental difficulty. This is because the 5 eV bond energy (BE) of an Al−O bond (in an Al−O−O−Al fragment) is equivalent to the energy necessary to cleave the O−O bond in the O_2 molecule, producing two O atoms (the O_2 BE is 5.16 eV).[2] A peroxo intermediate fragment Al−O−O−Al, containing two Al−O bonds, will therefore be highly excited (5 eV excess energy) and thus O atoms can also be ejected from the surface.[8] In order to avoid such difficulties, mainly O_2 reactions with surfaces of noble metals have been investigated. There, the M−O bond energy is much smaller (e.g., for Pd−O, 2.87 eV from $PdO_{(g)}$[2] and for Pt−O, 3.28 eV[9a]), and therefore it is possible to detect intermediate fragments, for example, Pt−O−O−Pt, with microscopic methods.[9−11]

Besides the investigations of the hindered O_2 reactions with metal surfaces by using microscopic methods (AFM, STM), a further experimental approach, namely, mass spectrometric investigations of metal atom clusters and their O_2 reactions, promises to give a deeper insight into this complex reaction mechanism.

$Al_n^\pm$ clusters have been investigated in many experimental and theoretical papers during the last two decades.[6,13−16] However, only the Al_{13}^- cluster appears to be an ideal molecular model for studying reactions involving bulk metals. The surprising similarity for the chlorination of the Al_{13}^- cluster and Al metal illustrates the similar thermodynamic behavior.[12,13]

$$Al_{13}^- + 3Cl_2 \rightarrow Al_{11}^- + 2AlCl_{3(g)}$$

$$\Delta_R H = -1137 \text{ kJ mol}^{-1} \quad \text{(calcd)}$$

$$2Al_{(s)} + 3Cl_2 \rightarrow 2AlCl_{3(g)}$$

$$\Delta_R H = -1166 \text{ kJ mol}^{-1} \quad \text{(expt)}$$

However, for the observed hindered reaction of the Al_{13}^- cluster with O_2, note that also the reaction of O_2 with bulk Al is unexpectedly slow,[7,15,18] there have been given several different explanations: (1) the outstanding electronic stability of Al_{13}^- with its 40 valence electron jellium core,[17] (2) the exceptional geometry in which a central Al atom is surrounded by 12 additional Al atoms, which form an icosahedron around it, that is, a magic geometry, (3) the outstanding electron affinity (3.6 eV) of Al_{13}, which is as large as that of the atomic chlorine atom, and finally (4) the spin-forbidden reaction of triplet O_2 with the singlet Al_{13}^- species to give singlet Al_9^- and $2Al_2O$.[18−21]

It was demonstrated that isolated Al_{13}^- ions in an O_2 atmosphere of about 10^{-8} mbar in an ion cyclotron resonance (ICR) trap do not form Al_9^- species even after about 600 s.[18] In order to show that this hindered $Al_{13}^- + O_2$ reaction is not just a special case but is of general interest, we measured the rate coefficients of O_2 reactions with a number of Al_x^- clusters near the Al_{13}^- species with closed- and open-shell structure. We found slow reactions for Al_9^-, Al_{11}^-, and Al_{13}^- and comparatively fast reactions for Al_8^-, Al_{10}^-, Al_{12}^-, and Al_{14}^-. The doublet character of the last four species eliminates hindrances caused by the violation of the spin conservation rule and allows one to compare these rate coefficients with those of the spin-allowed Cl_2 reactions. In order to show the importance of this rule, O_2 reactions with $Al_{13}H^-$ (open shell) and $Al_{14}H^-$ (closed shell) are also investigated. In an ongoing investigation, we study the acceleration of the $Al_{13}^- + O_2$ reaction by increasing the collisional energy. The experimental findings and the analysis of these complex results are the subject of a further publication.[22]

To further study the general importance of the O_2 + metal reaction, we have extended our investigation to a number of Ga_x^- clusters. Though Ga is a homologue of Al, it exhibits many differences: Unexpectedly, the electronegativity (EN) of Ga, at 1.8, is higher than that of Al (1.5). Ga has seven crystalline modifications; these vary in their bond formation from covalent bonding as in the case of boron toward metallic bonding as in a real metal. The α-Ga modification, with one short Ga−Ga bond, often is called a molecular metal,[1,15] a property that is also reflected in its low melting point of 28 °C. Also, true metal structures like Ga(IV) are observed under high pressure.[15,23,24] However, the electronic behavior of naked Ga_x^- should be similar to that of Al_x^- clusters since the same number of valence electrons are involved in bonding, for example 40 in the jellium-like Ga_{13}^- cluster. Therefore, while reactions of O_2 with Ga_x^- clusters should be electronically similar to reactions with Al_x^- clusters, they are different from a thermodynamic point of view, because the Ga−O bond energy is considerably smaller than that of Al−O. The Al−O bond strength is much larger, however, than that of all noble metal−oxygen bonds, as the following comparison shows: Al−O = 5.35 eV (from Al_2O), Ga−O = 4.59 eV (from Ga_2O), and Pd−O = 2.87 eV (from $Pd{-}O_{(g)}$).[2] Accordingly, the mass spectrometric results for the Ga_x^- clusters presented here can be expected to show whether the model for the $Al_x^- + O_2$ reactions is valid for other metals that exhibit different thermodynamic properties. The different thermodynamic properties of Ga compounds in comparison to Al compounds are also reflected in procedures for forming Ga_x^- and Al_x^- clusters. While Al_x^- clusters were formed by laser desorption of solid $LiAlH_4$, Ga_x^- species can be obtained after laser irradiation of solid GaN, which will be described here for the first time.[2,25,26]

The rate coefficients presented in this work were determined by bringing either single-sized clusters or a collection of clusters with different sizes into reaction with O_2 under (nearly) single-collision conditions (10^{-8} mbar). This means that the reaction products are generally detected before a second collision with O_2 occurs. This approach is essential in order to study the single elementary steps of the reaction. In contrast, in recent flow tube experiments by other authors at about 0.5 mbar, up to 100 collisions between O_2 and a single cluster occur before the products are detected.[11] In these experiments, rate coefficients of O_2 with a large number (ca. 50) of Al_x^- clusters of different size

dx.doi.org/10.1021/ja4125548 | J. Am. Chem. Soc. 2014, 136, 3607−3616

were estimated via a data analysis based on a Monte Carlo model.[20,21]

A comparison of measured rate coefficients with predictions from kinetic theories would allow further conclusions regarding the underlying reaction mechanisms. However, the calculation of rate coefficients from first principles with molecular and transition state data from quantum chemical methods requires a reliable knowledge of barrier heights. For the reactions of $^3O_2$ with closed- and open-shell Al_x^- and Ga_x^- clusters, these calculations are complicated not only by failure of single-determinant methods but also by the existence of multiple isomeric intermediates.[27]

On the basis of our experimental results and supported by DFT calculations, we obtained evidence for a model in which the peroxo intermediate $[M_x\cdots O_2]^-$, as the earliest species along the reaction coordinate that exhibits a typical arrangement of valence electrons, plays an essential role. This peroxo intermediate is also the prominent species in a more general, hypothetical reaction scheme that is, a Gedanken experiment, which should allow predictions to be made for O_2 reaction rates of any metal atom clusters. Within this broader scheme, the oxidation of the M_x^- cluster to a M_x^+ species with simultaneous reduction of O_2 to the O_2^{2-} peroxo moiety plays the major role.[28,1]

RESULTS AND DISCUSSION

Mechanisms and Rate Coefficients. Prior to the determination of rate coefficients, we studied qualitatively the reaction pattern of all $M_{m/n}^-$ clusters (m = even-numbered; n = odd-numbered; M = Al, Ga) with O_2. The clusters were first isolated and brought to collision with oxygen at a pressure of about 4×10^{-8} mbar for several seconds. Let us consider Ga_m^- cluster anions first. For these even-numbered clusters (Ga_{10}^-–Ga_{28}^-), the following spontaneous reactions were observed.[29]

$$Ga_{10}^- + O_2 \rightarrow Ga_6^- + 2Ga_2O$$

$$Ga_{10}^- + O_2 \rightarrow Ga_5^- + Ga_2O + Ga_3O$$

$$Ga_{12}^- + O_2 \rightarrow Ga_7^- + Ga_2O + Ga_3O$$

$$Ga_{14}^- + O_2 \rightarrow Ga_{10}^- + 2Ga_2O$$

$$Ga_{16}^- + O_2 \rightarrow Ga_{12}^- + 2Ga_2O$$

$$Ga_{16}^- + O_2 \rightarrow Ga_{11}^- + Ga_2O + Ga_3O$$

$$Ga_{18}^- + O_2 \rightarrow Ga_{13}^- + Ga_2O + Ga_3O$$

$$Ga_{20}^- + O_2 \rightarrow Ga_{16}^- + 2Ga_2O$$

$$Ga_{20}^- + O_2 \rightarrow Ga_{15}^- + Ga_2O + Ga_3O$$

$$Ga_{22}^- + O_2 \rightarrow Ga_{18}^- + 2Ga_2O$$

$$Ga_{24}^- + O_2 \rightarrow Ga_{20}^- + 2Ga_2O$$

$$Ga_{26}^- + O_2 \rightarrow Ga_{22}^- + 2Ga_2O$$

$$Ga_{28}^- + O_2 \rightarrow Ga_{24}^- + 2Ga_2O$$

In contrast to all these spontaneous reactions, the odd-numbered, closed-shell Ga_n^- clusters react at least one order of magnitude more slowly with O_2, and only upper limits to the rate coefficients can be given.[30]

For the corresponding $Al_{m/n}^-$ clusters, qualitatively the analogous reactions were observed that is, spontaneous reactions for even-numbered Al_m^- clusters with formation of $Al_{(m-4)}^-$ or $Al_{(m-5)}^-$ fragments. Odd-numbered Al_n^- clusters were found to be much less reactive, Al_{13}^- and Al_9^- being nearly stable in agreement with our former observations[18] and those of Castleman et al.[21]

For the determination of rate coefficients, O_2 was admitted to the ICR cell by a manual leak valve (Varian) allowing us to maintain a constant partial pressure of 3×10^{-10} to 4×10^{-8} mbar in the cell. Note that with this method the maximum pressure was limited to $\sim 4 \times 10^{-8}$ mbar, because ion detection took place while the reaction gas (O_2) was present in the ICR cell. Rate coefficients for all $Ga_{m/n}^-$ clusters are shown in Figure 1.

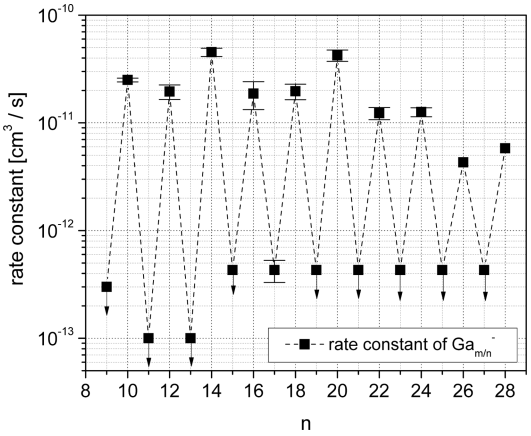

Figure 1. Measured rate coefficients for reactions of $Ga_{m/n}^-$ clusters with O_2. Error bars originate from at least two independent measurements carried out on different days. For numerical values of Ga_9^-, see Table 2.

By knowing the reaction behavior of some single-sized clusters M_n^- (see above), we were also able to study and characterize the reactivity of a whole collection of differently sized clusters (e.g., Ga_{11}^-–Ga_{28}^-) at once and to numerically fit the integrated rate equations of the consecutive reaction steps to the experimental data to obtain pseudo-first-order rate coefficients, k_i (see Supporting Information). For these calculations, the software *DetMech*[31] was used.

Since for several cluster types the rate coefficient k_i was determined by isolating the single clusters first (e.g., Ga_{10}^-, Ga_{13}^-, Ga_{22}^-, and Al_{13}^-), the reliability of the collective measurements has been confirmed because values from both measurements agree well.

In order to derive reliable reaction rates of the $M_{m/n}^-$ clusters, all ion intensities were normalized to the intensity of Ga_9^-. This is justified because (1) the rate coefficient of M_9^- with O_2 is much smaller (about a factor of 100) compared with the other (even-numbered) clusters and (2) there is no cluster that reacts to give M_9^- because for Al_{13}^- and Ga_{13}^-, even at prolonged reaction times of up to 600 s, no reaction with O_2 was observed (cf. above).

In order to generate $Al_{m/n}H^-$ clusters, the $Al_{m/n}^-$ clusters were exposed to a hydrogen atmosphere at 10^{-6} mbar for 1–3 s.[18]

Model for the Primary, Rate-Determining Step. The overall reactions of Al_x^- and Ga_x^- clusters with O_2 are exemplarily summarized for Al_x^- clusters in the following equations, which are divided into spin-forbidden (2a) and spin-allowed reactions (2b):

odd-numbered clusters

$$^1Al_n^- + {}^3O_2 \rightarrow {}^1Al_{n-4}^- + 2{}^1Al_2O \qquad (2a)$$

dx.doi.org/10.1021/ja4125548 | J. Am. Chem. Soc. 2014, 136, 3607–3616

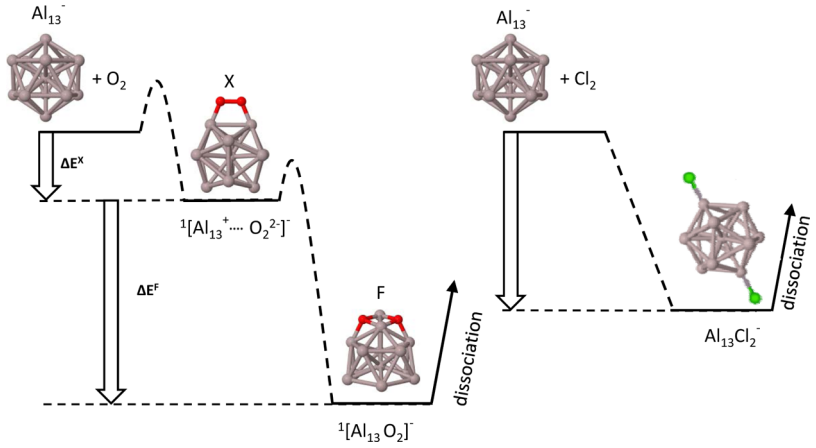

Figure 2. (left) Schematic presentation of the reaction path of an $Al_{n/m}^-$ cluster with $^3O_2$. As a spin-forbidden example, the hindered reaction of the Al_{13}^- cluster is shown: Al_{13}^- reacts via spin transition to the peroxo-bonded O_2^{2-} intermediate **X** ($^1Al_{13}^- + {}^3O_2 \rightarrow {}^1[Al_{13}^{+}\cdots O_2^{2-}]^-$) (energy gain ΔE^X) and finally to the more stable anion **F**, $^1[Al_{13}O_2]^-$ (ΔE^F) corresponding to complete oxidation of the Al_{13}^- cluster with a single O_2 molecule (cf. text). (right) Spontaneous reaction of Al_{13}^- cluster with Cl_2 to the completely oxidized $[Al_{13}Cl_2]^-$ intermediate, which rapidly decomposes to Al_{11}^- + 2AlCl.[33]

Table 1. Calculated (DFT) Values of ΔE^X and $\Delta E^X + \Delta E^F$ (eV) for the Energy Gain from the Reactants (e.g., $Ga_{13}^- + {}^3O_2$) to the Side-on Bonded Intermediate X (e.g., $[Ga_{13}^{+}\cdots O_2^{2-}]^-$) and to the Ground State F (e.g., $[Ga_{13}O_2]^-$)[a]

	Ga_9^-	Ga_{10}^-	Ga_{11}^-	Ga_{12}^-	Ga_{13}^-	Ga_{14}^-	Al_{13}^-	Al_{14}^-
$-\Delta E^X$	1.84	1.92	1.87	1.83	1.14	2.1	2.21	3.1
$-\Delta E^X + -\Delta E^F$	4.58	5.45	4.62	4.73	4.64	5.12	6.99	8.10

[a]For explanation, see Figure 2.

even-numbered clusters

$$^2Al_m^- + {}^3O_2 \rightarrow {}^2Al_{m-4}^- + 2{}^1Al_2O \qquad (2b)$$

Note, however, that this four electron reaction[32] is only the simple summarization of a very complex reaction route in which many intermediates are involved. Since quantum chemical calculations of the complex potential energy surface (PES) for the $Al_x^- + O_2$ reactions are not expected to give reliable results for transition states, we tried to develop a plausible model by correlating our measured rate coefficients with the potential energies of stable and metastable species. Additional information is gained from the different reaction rates of Al_x^- clusters with Cl_2 and with O_2 if no spin transition occurs. From our DFT calculations, it follows that the first well-defined intermediate in every $Al_{n/m}^- + O_2$ reaction is a $[Al_{n/m}^{+}\cdots O_2^{2-}]^-$ species (in the following denoted by **X**) in which a peroxo (O_2^{2-}) group is polar-bonded to the $Al_{n/m}^-$ cluster via two oxidized Al atoms (Al^+). In Figure 2, the situation is exemplified for $Al_{13}^- + O_2$, with $^1[Al_{13}^{+}\cdots O_2^{2-}]^-$ as the intermediate **X**. Note that in the following, the stabilization energy of **X** with respect to the reactants is denoted by ΔE^X. For all even-numbered Al_m^- clusters, this intermediate **X** is in a doublet state and formed without spin restrictions; for the odd-numbered clusters Al_n^-, however, **X** is in a singlet state, and a spin flip is necessary.

The peroxo moiety O_2^{2-} within these intermediates (also present in H_2O_2, for example),[1] bonded to two different metal atoms of the cluster, represents a chemically well-known situation with classical bonding,[28] which is isoelectronic to that of the F_2 molecule. Therefore, an intermediate **X** of this type can be expected to have a pronounced local minimum on the PES in accordance with our DFT results.

Thus, the $[Al_{n/m}^{+}\cdots O_2^{2-}]^-$ intermediate **X** with its local energy minimum ΔE^X (Table 1) corresponds to the first well-defined step along the reaction route, where the O_2 molecule has obtained two electrons from the $Al_{n/m}^-$ cluster. The $[Al_{n/m}^{+}\cdots O_2^{2-}]^-$ intermediate has O_2 bonded side-on, bridging between two aluminum atoms. With the transfer of two electrons, the $Al_{n/m}^-$ cluster is oxidized to an $Al_{n/m}^+$ unit, and the O−O bond distance is elongated becoming an O−O single bond in the O_2^{2-} moieties, the normal octet of electrons is maintained on each oxygen atom. This $[Al_{n/m}^{+}\cdots O_2^{2-}]^-$ intermediate reflects just the first step of the complete reaction with a four-electron transfer to two bridging O^{2-} ions of the final $[Al_{n/m}O_2]^- = [Al_{n/m}^{3+}\cdots 2O^{2-}]^-$ dioxide cluster **F** (Figure 2), which represents the global minimum.

Under high-vacuum conditions, collisional stabilization of the vibrationally excited dioxide $[Al_{n/m}O_2]^-$ cluster **F** (see Table 1) can be neglected because a low-lying decomposition channel giving $Al_{n/m-4} + 2Al_2O$ exists (Figure 3).[34] As illustrated in Figure 2 and discussed in the following, it is probably not the formation of this final, highly vibrationally excited dioxide cluster **F**, ($\Delta E^X + \Delta E^F$), that determines the overall rate constant but instead, the formation of the above-mentioned peroxo-bonded $[Al_{m/n}^{+}\cdots O_2^{2-}]^-$ intermediate **X** (Figure 2) with a much lower energy gain ΔE^X in the range of 2−3 eV. The calculated energies of the ground state **F** and the intermediate **X** of all $Al_{n/m}^-$ and $Ga_{n/m}^-$ clusters under discussion are listed in Table 1, and the corresponding structures are presented in the Supporting Information.

This conclusion is supported by our previous investigations on (spin-allowed) reactions of Al_{13}^- with Cl_2, in which Al_{11}^- and 2AlCl molecules are formed spontaneously via decomposition of the excited $[Al_{13}Cl_2]^-$ cluster and which are faster (3−6 times)[6,33] than those of the even-numbered Al_m^-/Ga_m^- clusters with O_2, which are also spin-allowed.

Despite the smaller energy gain in forming the most stable oxidized cluster (4.5 eV for $Al_{13}^- + Cl_2 \rightarrow [Al_{13}Cl_2]^-$ compared with 7 eV for $Al_{13}^- + O_2 \rightarrow [Al_{13}O_2]^-$), the overall reaction $Al_{13}^- + Cl_2$ is faster than the overall reaction $Al_{13}^- + O_2$. From this observation, we conclude that for the $Al_{m/n}^- + O_2$ reactions, a less excited intermediate is likely to exist that determines the rate

dx.doi.org/10.1021/ja4125548 | J. Am. Chem. Soc. 2014, 136, 3607−3616

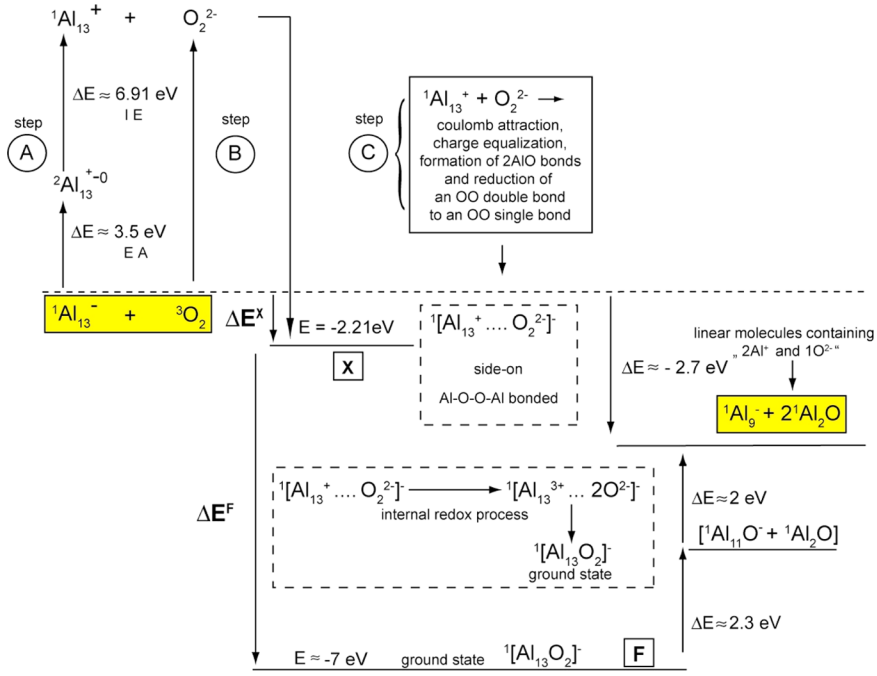

Figure 3. A schematic energy cycle of the $^1Al_{13}^- + {}^3O_2$ reaction (reactants and final products are yellow; see text). In order to understand the formation of the side-on bonded intermediate $[Al_{13}^+\cdots O_2^{2-}]^-$, **X**, (Figure 2) an alternative route via a hypothetical set of steps A, B, and C is constructed. The multistage process from the $^1[Al_{13}^+\cdots O_2^{2-}]^-$ intermediate to the ground state $^1[Al_{13}O_2]^-$, species **F**, (Figure 2) and its subsequent decomposition to the observed Al_9^- cluster is simplified. The primary reaction of the reactants proceeds via a weakly bonded charge/induced dipole complex (not shown) and a spin transition barrier (not shown) to the peroxo intermediate $[Al_{13}^+\cdots O_2^{2-}]^-$, **X**. Its energy corresponds to the value of $\Delta E^X = E(\mathbf{A}) + E(\mathbf{B}) + E(\mathbf{C})$.

Table 2. Experimentally Determined Rate Coefficients $[10^{-11}$ cm^3 s$^{-1}]$[a]

	Ga_9^-	Ga_{10}^-	Ga_{11}^-	Ga_{12}^-	Ga_{13}^-	Ga_{14}^-	Ga_{15}^-	Ga_{16}^-
	0.03[b]	2.5 ± 0.1	0.01[b]	2.0 ± 0.3	0.01[b]	4.5 ± 0.4	0.04[b]	1.9 ± 0.5
Al_8^-		Al_{10}^-		Al_{12}^-		Al_{14}^-		Al_{16}^-
8.8 ± 3.9		6.0 ± 0.6		3.0 ± 0.3		4.5 ± 0.6		4.2 ± 0.9

[a]The given error is derived from at least two independent measurements. Note that the absolute error is estimated to be on the order of ±50% and is mainly due to uncertainties of the pressure measurement. [b]Only the upper limit could be determined.

of the overall reaction. From our quantum chemical calculations, it follows that this intermediate is the peroxo species, **X**, $[Al_{m/n}^+\ldots O_2^{2-}]^-$.

On the basis of these arguments, we propose the following general model for the $Al_{m/n}^- + O_2$ reaction: The energy gain ΔE^X for the formation of the peroxo intermediate determines the overall rate of reaction. The larger the energy gain, the larger the rate coefficient. This could be a manifestation of the Evans–Polanyi principle (see e.g., ref 35). If the reaction is spin-forbidden, the rate is slowed down.

The High Reactivity of the Even-Numbered Al_m^- and Ga_m^- Clusters. In order to verify the above-mentioned model, we examined first the open-shell gallium clusters Ga_{10}^-, Ga_{12}^-, and Ga_{14}^-, for which the rate coefficients can be determined more accurately than for the similar Al_{10}^-, Al_{12}^-, and Al_{14}^- clusters. This is because the intensities and particle densities of the $Ga_{n/m}^-$ clusters are higher than those for the $Al_{n/m}^-$ clusters due to their different formation process. In any case, the reactions of even-numbered Al_m^- and Ga_m^- clusters with $^3O_2$ are spin-allowed (cf. eq 2b) and therefore can proceed spontaneously, which is confirmed by our experiments. The experimentally determined rate coefficients are displayed in Figure 1 and collected in Table 2.

Clearly, the rate coefficients increase in the sequence, $Ga_{12}^- \approx Ga_{16}^- < Ga_{10}^- < Ga_{14}^-$. Even accounting for absolute errors, the measured rate coefficients are below the Langevin limit by a factor of 20, this limit being on the order of 5×10^{-10} cm^3 s^{-1} for the $Ga_{m/n}^- + O_2$ reactions (polarizability of O_2 = 1.58×10^{-30} cm^3).[36] Obviously, the capture of O_2 by the cluster ion (ion/induced dipole interactions) is not the rate-determining step, and an energy barrier or an entropic bottleneck, in the case of the even-numbered clusters, between a weakly bound charge/induced dipole complex and the more stable $[Ga_m^+\cdots O_2^{2-}]^-$ intermediate is likely to exist. This conclusion is supported by the approximately two times faster, more exoergic O_2 reaction of Al_m^- clusters versus the analogous Ga_m^- clusters (see Table 2).[37] This is strong evidence for explaining the origin of the different rate coefficients of Al_m^- and Ga_m^- clusters. The rate-determining formation of the peroxo intermediate $^2[M_m^+\cdots O_2^{2-}]^-$ is more exoergic (ΔE^X) for the Al_m^- clusters; that is, more energy (about 1 eV) is gained for Al_{14}^- than for Ga_{14}^-. Obviously, a correlation exists between the measured rate coefficient and the calculated ΔE^X values.

Assuming a similar reaction mechanism for the different Ga_m^- clusters, the Ga_{10}^- cluster should react somewhat faster than Ga_{12}^-, and Ga_{14}^- should react significantly faster than Ga_{10}^- and Ga_{12}^-, which is in line with the experimental observation of the

dx.doi.org/10.1021/ja4125548 | J. Am. Chem. Soc. 2014, 136, 3607–3616

reaction rates (see preceding); that is, the Ga_{14}^- cluster exhibits the highest reactivity of all even-numbered Ga_m^- clusters because of its high exoergicity for the formation of the rate-determining peroxo intermediate, **X**, for example, 2.1 eV for $[Ga_{14}^+\cdots O_2^{2-}]^-$.

This interpretation is surprisingly supported by kinetic investigations of the O_2 reactions with alkyl radicals,[38] a completely different reaction system. As can be seen from Table 3, for both reactions (with open-shell Ga_m^- clusters and alkyl radicals), not only are the absolute rate coefficients very similar, but also a correlation is seen between the rate coefficients and the exoergicity of the association step.

Table 3. Experimental Rate Coefficients and Calculated Exoergicity for Selected $^2Ga_m^-$ + O_2 and Alkyl Radical + O_2 Reactions[a]

cluster	$k/10^{-11}$ ($cm^3\ s^{-1}$)	ΔE^X (eV)	radical[38]	$k/10^{-11}$ ($cm^3\ s^{-1}$)	−BDE (eV)
Ga_{10}^-	2.5	−1.92	primary alkyl	0.8	−1.54
Ga_{12}^-	2.0	−1.83	secondary alkyl	1.2	−1.62
Ga_{14}^-	4.5	−2.10	tertiary alkyl	2.0	−1.68

[a]BDE, bond dissociation energy of the R−O_2 bond.[38]

The Low Reactivity of Odd-Numbered Al_n^- and Ga_n^- Clusters. The fast O_2 reactions of all even-numbered Ga_m^- clusters are in contrast to the hindered reactions of the odd-numbered Ga_n^- clusters with rate coefficients below the Langevin limit by a factor of >1000 (cf. Figure 1 and Table 2). Like in the case of the Al_{13}^- and Ga_{13}^- clusters, an energy barrier has to be overcome during which the spin transition proceeds. This barrier, as with the even-numbered Ga_m^- clusters, should depend also on the stability of the peroxo intermediate **X**, for example, $[M_{13}^+\cdots O_2^{2-}]^-$. For the Ga_{13}^- cluster, the energy gain for this side-on intermediate is −1.14 eV. Furthermore, also for adjacent odd-numbered Ga_n^- clusters, the relationship between ΔE^X and the rate coefficient can be expected to apply. For Ga_9^- and Ga_{11}^-, the following ΔE^X values are calculated: −1.84 and −1.87 eV (Table 2). From these more exoergic reactions, in comparison to Ga_{13}^- (−1.14 eV), a faster reaction than for Ga_{13}^- should be expected. But unfortunately, for each of these three clusters, the rate coefficient is too small to be measured exactly under our experimental conditions; that is, only an upper limit can be given. Moreover, since the situation for the O_2 reaction with Ga_{11}^- is unexpectedly complex (see Supporting Information), one should only compare Ga_9^- and Ga_{13}^-. Specifically, Ga_{13}^- exhibits the smallest and Ga_9^- the largest upper limit, which is at least in line with our proposed correlation.

Comparison of Even- and Odd-Numbered Clusters. So far it seems as if a consistent picture can be drawn within the series of odd- and even-numbered $Al_{n/m}^-$ and $Ga_{n/m}^-$ clusters in the limited size windows, Ga_9^- to Ga_{14}^- and Al_{13}^- to Al_{14}^-. Furthermore, this picture is also valid, if one compares the slowest and the fastest reaction of an even/odd cluster pair. The ΔE^X values for the formation of the peroxo intermediates **X** of Al_{13}^- and Al_{14}^- are −2.2 and −3.1 eV, respectively. For the analogous Ga_{13}^-/Ga_{14}^- pair, the following ΔE^X values are calculated: −1.14 and −2.1 eV, respectively. In the case of the Ga clusters, an increase of a factor of ∼400 is observed for the rate coefficients (Table 2).[39]

The moderate correlation between the ΔE^X values and the rate coefficients for the M_{13}^-/M_{14}^- pair gives a first indication that there must be an additional influence, besides energy, on the reaction rate. This assumption is confirmed by the following example, for which drastically different reaction rates are observed even though the ΔE^X values are similar. As shown above, there are fast spontaneous reactions for Ga_{10}^- and Ga_{12}^- with ΔE^X values of −1.92 and −1.83 eV, respectively. Though the ΔE^X values for Ga_9^- and Ga_{11}^- (−1.84 and −1.87 eV, respectively) are in the same range, the rate coefficients for the latter ones are about 100 times slower (see Table 2).

Obviously, there is a rate-decreasing process for the odd-numbered Ga_n^- clusters, because an accelerating process for the even-numbered Ga_m^- clusters can be ruled out.[40]

The spin-forbidden transition during the slow reaction of the odd-numbered clusters (e.g., singlet Al_{13}^- with $^3O_2$ toward the singlet $^1[Al_{13}^+\cdots O_2^{2-}]^-$ intermediate) should cause an additional increase of the barrier, which in a first approximation was discussed above, as being based only on the relatively low exoergicity ΔE^X of the reaction.

Therefore, the striking difference between the rate coefficients for the even- and odd-numbered clusters gives a strong indication that the hindered $^3O_2$ reaction with closed-shell clusters is based on an additional barrier caused by the spin transition.

Can Reactivities for Size-Similar Open- And Closed-Shell Clusters Be Estimated? Besides the special effect of the spin transition, which causes a dramatic decrease of the reaction rate, there is clearly a significant correlation between the $Al_{n/m}^-/Ga_{n/m}^-$ + O_2 reaction rates of different clusters and the energy gain ΔE^X from the educts to the peroxo intermediates, which have been calculated with DFT methods. Now the question arises whether it is possible to make a simpler prediction about the reactivity of such clusters based on the ΔE^X correlation.

In order to illustrate this approach, we have developed a thermodynamic cycle leading to the peroxo intermediate **X**, which is shown in Figure 3. Using the Al_{13}^- cluster as a prominent example, the cycle involves the reactants $^1Al_{13}^-$ and $^3O_2$, which react with a ΔE^X value of −2.21 eV (Table 2) to form **X**, $^1[Al_{13}^+\cdots O^{2-}]^-$.

This model process begins with the two-step oxidation (EA + IE) of Al_{13}^- to Al_{13}^+ (**A**) and the two-step reduction of $^3O_2$ to the singlet dianion O_2^{2-} (**B**) (isoelectronic to the F_2 molecule). Subsequently, the Coulomb attraction between Al_{13}^+ and O_2^{2-} and the formation of two Al−O bonds via charge neutralization proceed, releasing energy, and finally the $^1[Al_{13}^+\cdots O_2^{2-}]^-$ intermediate, **X**, is formed (**C**). Since during this whole process[41] step **C** is nearly the same for $Al_{m/n}^-$ and $Ga_{m/n}^-$ clusters, provided they are of similar size as those discussed in this paper (e.g., Ga_9^-, Ga_{11}^-, and Ga_{13}^- or Ga_{10}^-, Ga_{12}^-, and Ga_{14}^-), the energy gain ΔE^X calculated with DFT methods should be mainly reflected by the differences in step **A**. The energy values of step **A** for some $Al_{n/m}^-$ and $Ga_{n/m}^-$ clusters have been calculated and are collected in Table 4. These values mainly determine the ΔE^X values and therefore the rate coefficients (Figure 3): The smaller the value of $E(\mathbf{A})$ = EA + IE, the more negative the value of ΔE^X, as the exoergic formation of Ga−O/Al−O bonds, step **C**, will further exceed **A**.

In the following, we will concentrate on the Ga_m^- cluster reactions. First we look at the spontaneous reactions of Ga_{10}^-, Ga_{12}^-, and Ga_{14}^-. The reaction with Ga_{14}^- exhibits the largest rate coefficient. This property of Ga_{14}^- is in line with its smallest value of $E(\mathbf{A})$ (8.57 eV), while for the slower reaction of Ga_{12}^-, the largest value of $E(\mathbf{A})$ (8.87 eV) has been obtained. Therefore, as mentioned above, the values of $E(\mathbf{A})$ for the clusters Ga_{10}^-, Ga_{12}^-, and Ga_{14}^- are in line with the observed increasing reactivity toward O_2 of these Ga_n^- clusters: $Ga_{12}^- < Ga_{10}^- < Ga_{14}^-$.

dx.doi.org/10.1021/ja4125548 | J. Am. Chem. Soc. 2014, 136, 3607−3616

Table 4. Electron Affinities (EA, eV) and Ionization Energies (IE, eV) of Neutral $Al_{m/n}$ and $Ga_{m/n}$ Clusters (n/m = 9−14) Obtained from Our DFT Calculations

	$Al_{m/n}$			$Ga_{m/n}$		
m/n	EA	IE	[EA + IE][a]	EA	IE	[EA + IE][a]
9	2.76	6.37	9.13	2.87	5.94	8.81
10	2.67	6.42	9.09	2.47	6.24	8.71
11	2.84	6.24	9.08	2.79	6.37	9.17
12	2.78	6.39	9.17	2.58	6.29	8.87
13	3.50	6.91	10.41	3.29	6.10	9.39
14	2.61	5.95	8.56	2.42	6.15	8.57

[a]This value corresponds to **A** in Figure 3.

This simple ionic model is also in line with the reactivity of the closed-shell clusters Ga_9^-, Ga_{11}^-, and Ga_{13}^-. The largest value of $E(\mathbf{A})$ is obtained as expected for Ga_{13}^-, which is in line with the lowest reactivity. The Ga_{11}^- cluster should exhibit a higher reactivity than the Ga_{13}^- cluster, and the Ga_9^- cluster should show the highest reactivity of these three species. Though the experiments result in a similar reactivity of Ga_{13}^- and Ga_{11}^- with respect to the upper limits, this rough prediction without the consideration of the spin transition for the three clusters at least seems to reflect the principal trend. Thus, within the series of even-numbered and odd-numbered clusters, the simple ionic model is in line with experiments as well as with the results of DFT calculations.

Consequences from the Predicted Reactivity Based on the Ionic Model: Spin Transition Causes an Additional Hindrance. What about the validity of this simple model if one compares even- and odd-numbered Al_x^-/Ga_x^- clusters?[42] The difference, $\Delta E(\mathbf{A})$, of the $E(\mathbf{A})$ values (Figure 3, Table 4) for Ga_{13}^- and Ga_{14}^- ($\Delta E(\mathbf{A})$ = 9.39 − 8.57 eV = 0.82 eV) corresponds to a strong increase in the O_2 reactivity from Ga_{13}^- to Ga_{14}^- by over three orders of magnitude. The acceleration of the reaction is less prominent from Ga_{11}^- to Ga_{12}^- ($\Delta E(\mathbf{A})$ = 0.3 eV) and the smallest difference is to be expected for the pair Ga_9^- to Ga_{10}^- ($\Delta E(\mathbf{A})$ = 0.1 eV). However, since even the low value of $\Delta E(\mathbf{A})$ = 0.1 eV is contrasted by an observed increase in the O_2 reactivity from Ga_9^- to Ga_{10}^- of about two orders of magnitude, there must be an additional factor that will be responsible for this large difference in the reaction rates. Furthermore, even the large $\Delta E(\mathbf{A})$ value between Ga_{13}^- and Ga_{14}^- may be not sufficient to explain the strongly different reaction rates between the slowest (Ga_{13}^-) and the fastest (Ga_{14}^-) reacting cluster alone. Consequently, there has to be a further factor that decreases the reaction rate of the odd clusters (Ga_9^-, Ga_{11}^-, Ga_{13}^-) so drastically. This contribution, as discussed above, can only be the hindered spin transition, which, for example, makes the Ga_{13}^- + O_2, as well as the Al_{13} + O_2, reaction extremely slow.

The Reactivity of $Al_{13}H^-$ and $Al_{14}H^-$ Clusters. All in all, our proposed model seems to be on solid ground. Nevertheless, we expand our discussion to two hydrogen-containing Al clusters, which already had given strong experimental indications of the essential influence of the spin conservation rule.[18,20] If one H atom is added, then also one electron is added to the cluster, and consequently, the O_2 reactivity changes dramatically. The $Al_{13}H^-$ species as an open-shell cluster is highly reactive in contrast to the inert Al_{13}^- cluster, and the $Al_{14}H^-$ closed-shell cluster is strongly unreactive in contrast to the fast reaction of Al_{14}^-. We have roughly verified this change, which has been shown experimentally for $Al_{13}H^-$ and $Al_{14}H^-$,[18] by DFT calculations. A detailed discussion would require a separate paper, since many isomers have to be included for these Al_nH^- clusters in which the H atom can easily migrate on the cluster surface.[43] Therefore, only a small number of isomers ($Al_{13}H^-/[Al_{13}H\cdots O_2]^-/Al_{13}HO_2^-$ and $Al_{14}H^-/[Al_{14}H\cdots O_2]^-/Al_{14}HO_2^-$) were considered in our calculations. As was the case in the hydrogen-free clusters, energy gains were seen when going from reactants to the intermediate **X** and again going from **X** to the final product **F**. Some results are listed in the Supporting Information, from which the following conclusion can be drawn: The ΔE^X and the ΔE^F values are similar to those of the H-free clusters Al_{13}^- and Al_{14}^-. Therefore, these results once more confirm that it is not the formation of the highly excited species **F** but instead the formation of the intermediate **X** that determines the O_2 reaction rate. Furthermore, these results are in line with the conclusion that the spin conservation rule is responsible for the different reactivity of the open-shell and the closed-shell $Al_{n/m}^-$ and $Al_{n/m}H^-$ clusters with $^3O_2$.

CONCLUSION AND OUTLOOK

In order to understand the slower reactions of Al_x^- clusters with O_2 compared with their fast reactions with Cl_2, we have investigated a number of spin-allowed and spin-forbidden O_2 reactions with Al_x^- clusters in the size neighborhood of the Al_{13}^- cluster. Furthermore, we have extended our investigations to similar Ga_x^- clusters to examine whether our results are restricted to Al or are also valid for other metal atom clusters, as well as for the oxidation of metal surfaces in general. Accordingly, rate coefficients of the reactions of O_2 with Al_x^- and Ga_x^- (x = 9−14) near the size of the exceptional M_{13}^- have been measured by FT-ICR mass spectrometry under single collision conditions, that is, subsequent fast unimolecular reactions proceed before the next collision occurs. These measurements, which quantify the even/odd properties of these clusters, in particular, the fast reaction of the even-numbered, open-shell clusters and the slow, spin-forbidden reactions of the odd-numbered, closed-shell clusters, have been complemented by DFT calculations in which we have computed the ground state energies of the reactants, the intermediates, and the products. These results provide guidelines for the discussion of the experimentally determined rate coefficients. The critical intermediate that determines the reaction rate has a normal valence bonding character, because it contains the well-known peroxo unit $(O-O)^{2-}$, which is bonded to two neighboring metal atoms on the surface of the M_x^- cluster, after it is partially oxidized to a M^+ cluster. Simultaneously, the O_2 molecule is reduced to the O_2^{2-} moiety. The energy gain, ΔE^X, during formation of this $[M_x^+\cdots O_2^{2-}]^-$ intermediate is correlated to the rate coefficient of the M_x^- + O_2 reaction. The larger ΔE^X, the larger is the rate coefficient observed (for the spin-allowed reactions). This fundamental conclusion is furthermore supported by (a) the faster O_2 reactions of the Al_x^- clusters in comparison to the Ga_x^- clusters, because the formation of Al−O bonds is more exothermic than the formation of Ga−O bonds, and (b) the spin-allowed reaction of Al_x^- clusters with Cl_2 being faster than the spin-allowed reactions with O_2. This result is in line with our model if in reactions with chlorine, the formation of the highly excited dichloride cluster $Al_xCl_2^-$ is the rate-determining step (e.g., $Al_{13}Cl_2^-$ is excited with 4.5 eV and reacts to give Al_{11}^- + 2 AlCl) and if in reactions with oxygen the intermediate **X** (e.g., $[Al_{14}^+\cdots O_2^{2-}]^-$ with 3.1 eV) represents the critical, rate-determining species.

However, the energy of this intermediate $[M_x^+\cdots O_2^{2-}]^-$ cannot, by itself, completely account for the experimental findings regarding the reactivity of similar even- and odd-numbered

dx.doi.org/10.1021/ja4125548 | J. Am. Chem. Soc. 2014, 136, 3607−3616

clusters (e.g., Ga_{13}^- and Ga_{14}^-). The spin transition during the reaction of the odd-numbered cluster causes an additional hindrance for the $^3O_2$ reaction. This conclusion has been convincingly confirmed in calculations related to the recent experimental results for the H-containing clusters $Al_{13}H^-$ and $Al_{14}H^-$. Though the ΔE^X values of the O_2 reactions with $Al_{13}H^-$ and Al_{13}^- as well as with $Al_{14}H^-$ and Al_{14}^- are very similar, the reactivity changes radically. The addition of one H atom turns spin-forbidden reactions into spin-allowed reactions and vice versa; thus rates of reactions with an even number of aluminum atoms are strongly increased, and rates of reactions with odd numbers of aluminum atoms are conversely strongly decreased.

Furthermore, we developed a model that allows us to make predictions on the trends in O_2 reactivity within a small number of similar metal atom clusters. In this simple model, the formal oxidation of the metal cluster anion, M_x^-, to the cluster cation (e.g., $Al_x^- \rightarrow Al_x^+$) determines the ΔE^X value and therefore is responsible for the differing reactivity of the clusters.

To summarize, the quantification of the rate coefficients for a small number of Al_x^- and Ga_x^- clusters in the size vicinity of the exceptional Al_{13}^-/Ga_{13}^- species in principle seems to allow a deeper insight into all reactions of O_2 with metal atom clusters and possibly also with surfaces of bulk metals;[7] that is, also small changes within the geometric structure of surfaces will change the reactivity. Therefore, our results may also be of fundamental interest for many catalytic processes on metal surfaces where the addition or substitution of a single atom can change the reactivity dramatically.

In our ongoing experiments, we plan to quantify the spin-forbidden reactions of O_2 with Al_{13}^- and Ga_{13}^- clusters via well-defined excitation of the clusters to overcome the reaction barrier during the spin transitions. These results will be published in a separate paper.[22]

EXPERIMENTAL SECTION

All experiments were carried out in a commercial FT-ICR mass spectrometer (Ion Spec, Ultima) equipped with a 7 T actively shielded magnet (Cryomagnetics, Oak Ridge, TN, USA). Since the experimental setup and methodology was described elsewhere in detail,[6,18,44−46] only the essentials are given here.

Negatively charged aluminum and gallium clusters ($Al_{m/n}^-$, $Ga_{m/n}^-$) were generated by laser desorption from $LiAlH_4$[6,44] and GaN, respectively,[25] where the commercial MALDI (matrix-assisted laser desorption/ionization) source of the FTICR-MS was used (nitrogen laser, λ = 337.1 nm, pulse energy = 300 μJ, pulse width ≈ 4 ns (FWHM)).

After cluster formation, the ions were transferred into a cylindrical ICR cell via a quadrupole ion guide. To ensure efficient ion trapping (gas assisted dynamic trapping) and translational cooling of the cluster ions, argon (Argon 6.0, basi Schöberl GmbH & Co. KG) was admitted into the cell with a pulsed valve (General Valve) at a pressure of around 1×10^{-5} mbar for ∼1 s.

For the study of ions with one particular mass-to-charge ratio (e.g., m/z = 351.77 for Al_{13}^-), the species were isolated by the SWIFT (stored waveform inverse Fourier transform) excitation technique.[47] A second thermalization step was carried out in some cases to prevent possible (re)excitation of the ions due to the isolation process and to ensure thermal conditions. Because the second thermalization step did not change the measured rate coefficient within the experimental error, we conclude that ion (re)excitation by the SWIFT method can be neglected.

QUANTUM CHEMICAL CALCULATIONS

The theoretical studies concerning the kinetics are analogous to those presented recently.[33] It should be noted that interpretation of experimentally observed rate coefficients by computations demand clear knowledge of the potential energy surface with accurate estimation of threshold energies of the various intermediates, which in turn depend on the computational method; therefore we use reaction energies as a guide to understand the reactivity of the various clusters presented here. All the calculations were performed using the generalized gradient approximation (GGA) within the framework of the DFT. The gradient-corrected exchange and correlation functionals due to Becke−Perdew were employed here.[48] Split valence basis set supplemented with polarization functions was used for all the atoms.[49] The computations were carried out using the Turbomole software.[49] In the self-consistent field (SCF) calculations, the density and energy tolerances were set to 10^{-6} e/bohr^3 and 10^{-6} hartree, respectively. In the geometry optimization, all the structural parameters were fully optimized without any symmetry constraints, with an energy convergence of 10^{-5} hartree and a maximum gradient of 10^{-4} hartree/bohr. The lowest and other higher energy isomers of all oxide clusters were obtained using an unbiased systematic structure search based on genetic algorithm method.[50,51] In this procedure, all the structures generated either through initial population or cross breeding were fully optimized without any constraints using the same methods mentioned above.

ASSOCIATED CONTENT

Supporting Information

Quantum chemical calculations, structures, and energies (eV) and further experimental details. This material is available free of charge via the Internet at http://pubs.acs.org.

AUTHOR INFORMATION

Corresponding Authors

matthias.olzmann@kit.edu
hansgeorg.schnoeckel@kit.edu

Notes

The authors declare no competing financial interest.

ACKNOWLEDGMENTS

This work was supported by the Karlsruhe Institute of Technology (KIT), Deutsche Forschungsgemeinschaft (DFG), and Fonds der Chemischen Industrie. This material is based in part on work supported by the Air Force Office of Scientific Research (AFOSR) under Grant Numbers, FA9550-11-1-0068 (K.H.B.) and FA9550-11-1-0171 (B.E.). K.H.B. and B.E. also thank the Defense Threat Reduction Agency (DTRA) for partial support under Grant Number HDTRA-1-12-1-007. B.K. acknowledges financial support from the BoR-RCS grant. This manuscript is dedicated to Peter Jutzi on the occasion of his 75th birthday and his outstanding contributions in main group organometallic chemistry.

REFERENCES

(1) (a) *Holleman-Wiberg, Inorganic Chemistry*; Academic Press: San Diego, London, 2001. (b) *Holleman-Wiberg, Lehrbuch der Anorganischen Chemie*, 102. erweiterte Auflage; Wiberg, N., Wiberg, E., Holleman, A., Eds; Walter de Gruyter: Berlin, New York, 2007.

(2) Binnewies, M.; Milke, E. *Thermodynamical Data of Elements and Compounds*; Wiley-VCH: Weinheim, Germany, 1999.

(3) Chase, M. W., Jr. *J. Phys. Chem. Ref. Data* **1998**, No. Monograph 9, 1−1951.

(4) Al_2O is also the essential gaseous molecule after the O_2 oxidation of Mg-doped Al_xMg^- cluster anions. Luo, Z.; Grover, C. J.; Reber, A. C.; Khanna, S. N.; Castleman, A. W., Jr. *J. Am. Chem. Soc.* **2013**, *135*, 4307−4313.

(5) If the Cl_2 partial pressure is low and the temperature of the Al metal is about 700 °C, AlCl molecules are formed first, which are afterwards oxidized to $AlCl_3$: $Al + {}^1/_2Cl_2 \rightarrow AlCl_{(g)}$; $AlCl_{(g)} + Cl_2 \rightarrow AlCl_{3(g)}$ (see ref 6).

(6) Burgert, R.; Schnöckel, H.; Olzmann, M.; Bowen, K. H., Jr. *Angew. Chem.* **2006**, *118*, 1505−1508; *Angew. Chem., Int. Ed.* **2006**, *45*, 1476−1479.
(7) (a) Ertl, G. *Reactions at Solid Surfaces*; John Wiley & Sons Inc.: Hoboken, NJ, 2009. (b) Carbogno, C.; Groß, A.; Meyer, J.; Reuter, K. O_2 Adsorption Dynamics at Metal Surfaces: Non-Adiabatic Effects, Dissociation and Dissipation. In *Dynamics of Gas-Surface Interactions: Atomic-level description of Elementary Processes*; Muiño, R. D., Busnengo, H. F., Eds.; Springer Series in Surface Sciences; Springer: Berlin, 2013; Vol. *50*, pp 389−419.
(8) (a) Brune, H.; Wintterlin, J.; Behm, R. J.; Ertl, G. *Phys. Rev. Lett.* **1992**, *68*, 624. (b) Österlund, L.; Zoric, I.; Kasemo, B. *Phys. Rev. B* **1997**, 15452. (c) Sasaki, T.; Ohno, T. *Surf. Sci.* **2000**, *454*−*456*, 337−340. (d) Carbogno, C.; Behler, J.; Groß, A.; Reuter, K. *Phys. Rev. Lett.* **2008**, *101*, No. 096104.
(9) (a) Norman, J. H.; Staley, G.; Bell, W. E. *J. Phys. Chem.* **1967**, *71*, 3686. (b) Paglia, C.; Nilsson, A.; Hernass, B.; Karris, O.; Bennik, P.; Martensson, N. *Surf. Sci.* **1995**, *342*, 119.
(10) Based on the same arguments $Ag_nO_2^-$ species were detected in the gas phase during detailed mass spectrometric and theoretical investigations recently.[11]
(11) Luo, Z.; Gamboa, G. U.; Smith, J. C.; Reber, A. C.; Reveles, J. U.; Khanna, S. N.; Castleman, A. W., Jr. *J. Am. Chem. Soc.* **2012**, *134*, 18973.
(12) The similarity of the Al_{13}^- cluster to the bulk metal regarding thermodynamics is based on the very special electronic structure of this cluster (spherical jellium model with 40 valence electrons) as well as on its topological similarity concerning the coordination number. In both cases, a central Al atom is surrounded by 12 other Al atoms icosahedrally arranged in Al_{13}^- and cuboctahedrally arranged in the metal. Therefore, reactions of the Al_{13}^- are model reactions for those of the bulk metal, if the amount of energy necessary to remove two Al atoms from an Al_{13}^- cluster is compared with the energy change in the case of the bulk metal:[13] $Al_{13}^- \rightarrow Al_{11}^- + 2Al_{(g)}$, $\Delta_R H = +698$ kJ mol^{-1} (calcd); $2Al_{(s)} \rightarrow 2Al_{(g)}$, $\Delta_R H = +654 \pm 8$ kJ mol^{-1} (expt). Taking into account the usual error margin of DFT calculations, the energy needed for the removal of two Al atoms either from an Al_{13}^- cluster or from the bulk Al metal is almost identical. Here Al atoms form the energetically equivalent reference system, and therefore all reactions of Al_{13}^- clusters and Al metal should be very similar with respect to their energy balance.
(13) Burgert, R.; Schnöckel, H. *Chem. Commun.* **2008**, *18*, 2075−2089.
(14) Schnöckel, H. *Dalton Trans.* **2008**, *33*, 4344−4362.
(15) Schnöckel, H. *Chem. Rev.* **2010**, *110*, 4125−4163.
(16) (a) Jarrold, M. F.; Bower, J. E.; Kraus, J. S. *J. Chem. Phys.* **1987**, *86*, 3876−3885. (b) Jarrold, M. F.; Bower, J. E. *J. Am. Chem. Soc.* **1988**, *110*, 6706−6716. (c) Leuchtner, R. E.; Harms, A. C.; Castleman, A. W., Jr. *J. Chem. Phys.* **1989**, *91*, 2753−2754. (d) Leuchtner, R. E.; Harms, A. C.; Castleman, A. W., Jr. *J. Chem. Phys.* **1991**, *94*, 1093−1101. (e) Bach, S. B. H.; McElvany, S. W.; Wong, N. M.; Parent, D. C. *Chem. Phys. Lett.* **1993**, *209*, 57−62. (f) Hettich, R. L. *J. Am. Chem. Soc.* **1989**, *111*, 8582−8588.
(17) (a) de Heer, W. A. *Rev. Mod. Phys.* **1993**, *65*, 611. (b) Knight, W. D.; Clemenger, K.; de Heer, W. A.; Saunders, W. A.; Chou, M. Y.; Cohen, M. L. *Phys. Rev. Lett.* **1984**, *52*, 2141. (c) Cheng, H. P.; Berry, R. S.; Whetten, R. L. *Phys. Rev. B: Condens. Matter Mater. Phys.* **1991**, *43*, 10647−10653. (d) Ahlrichs, R.; Elliott, S. D. *Phys. Chem. Chem. Phys.* **1999**, *1*, 13−21.
(18) Burgert, R.; Schnöckel, H.; Grubisic, A.; Li, X.; Stokes, S. T.; Ganteför, G. F.; Kiran, B.; Jena, P.; Bowen, K. H. *Science* **2008**, *319*, 438−442.
(19) The hindered reactivity of O_2 with Al_{13}^- in a mixture of other Al_x^- clusters has been studied in recent papers, where also the unexpected stability has been discussed.[20,21]
(20) Reber, A. C.; Khanna, S. N.; Roach, P. J.; Woodward, W. H.; Castleman, A. W. *J. Am. Chem. Soc.* **2007**, *129*, 16098−16101.
(21) Woodward, W. H.; Eyet, N.; Shuman, N. S.; Smith, J. C.; Viggiano, A. A.; Castleman, A. W. *J. Phys. Chem. C* **2011**, *115* (20), 9903.
(22) Neumaier, M.; Olzmann, M.; Kiran, B., Bowen, K. H.; Burgert, R.; Schnöckel, H. manuscript in preparation.
(23) Schnepf, A.; Schnöckel, H. *Angew. Chem.* **2002**, *114*, 3683−3704; *Angew. Chem., Int. Ed.* **2002**, *41*, 3532−3554.
(24) Schnöckel, H.; Schnepf, A. *The Group 13 Metals Aluminum, Gallium, Indium and Thallium*; Aldridge, S., Downs, A. J., Eds.; Wiley: Chichester, U.K., 2011.
(25) The generation of Ga_x^- clusters via laser desorption of solid GaN has successfully been applied in our laboratory for many years. Koch, K. Metalloide Cluster in der Gasphase − FT/ICR-massenspektrometrische Untersuchungen, Dissertation, Universität Karlsruhe, 2005. However, this method has not been published before.
(26) The formation of Al_x^- clusters by irradiation of AlN was not successful, which seems plausible due to its higher thermodynamic stability; enthalpies of formation, $\Delta H^\circ_{f,298K}$(AlN) = −318 kJ mol^{-1}, $\Delta H^\circ_{f,298\ K}$(GaN) = −109 kJ mol^{-1}.[2]
(27) Obviously, because of these difficulties, controversial theoretical results have already been published: (a) Lu, Q. L.; Chen, L. L.; Wan, J. G.; Wang, G. H. *J. Comput. Chem.* **2010**, *31* (15), 2804−9. (b) Cooper, B. T.; Parent, D.; Buckner, S. W. *Chem. Phys. Lett.* **1998**, *284*, 401−406. (c) Hoshino, T.; Sekino, A.; Hata, M.; Tsuda, M. *Appl. Surf. Sci.* **20001**, *62*−*163*, 435−439. (d) Yuan, Q. H.; Li, J. B.; Fan, X. L.; Lau, W. M.; Liu, Z.-F. *Chem. Phys. Lett.* **2010**, *489*, 16−19.
(28) Though also superoxo-bonded (end-on) intermediates like that recently discussed for $Ag_{13}O_2$[11] are possible on the $Al_{13}^- + O_2$ PES, these species should be located in flat minima and exhibit a correspondingly short lifetime on their way to the peroxo species discussed here. This conclusion is plausible, since, as far as we know, in synthetic chemistry no molecules with an AOO constitution are known, where A represents a main group element. However, there are well-known examples for the normal valence AOOA peroxo arrangement (e.g., peroxosulfates and peroxophosphates).[1]
(29) The exoergic reactions of Ga_{10}^-, Ga_{12}^-, and Ga_{14}^- will be discussed in the text in more detail.
(30) Of all larger odd-numbered Ga_n^- clusters (with $Ga_n^- > Ga_7^-$), only Ga_{17}^- was found to react spontaneously with oxygen presumably because of the high stability of the Ga_{13}^- product: $Ga_{17}^- + O_2 \rightarrow Ga_{13}^- + 2Ga_2O$.
(31) Schumacher, E. *DETMECH − Chemical Reaction Kinetics Software*, University of Bern, 2003.
(32) Four Al atoms are oxidized to four Al^+ ions in the two Al_2O molecules. This picture of the oxidation of the outer ligand-bearing Al atom to monovalent Al^+ entities has been discussed on the basis of experiments with metalloid Al_nR_m ($n > m$) clusters,[1,14,15] and two O atoms of the O_2 molecules are reduced to two O^{2-} in the Al_2O species.
(33) Olzmann, M.; Burgert, R.; Schnöckel, H. *J. Chem. Phys.* **2009**, *131*, No. 174304.
(34) In contrast, if the pressure in the reaction cell is high, collisional stabilization of the cluster oxides $Al_{14}O^-$ and $Al_{15}O_2^-$ has been observed. Watanabe, T.; Tsukuda, T. *J. Phys. Chem. C* **2013**, *117*, 6664−6668.
(35) Levine, R. D. *Molecular Reaction Dynamics*; Cambridge University Press: Cambridge, U.K., 2005.
(36) *Handbook of Chemistry and Physics*, 75th ed.; Lide, D. R., Ed.; CRC Press: Boca Raton, FL, 1994.
(37) The rate coefficients of Al_8^-, Al_{10}^-, Al_{12}^-, and Al_{14}^- are about 20−50% smaller than those discussed by other authors from flow tube experiments and from a sophisticated estimation of rate coefficients;[21] however, their error margins are about 10 times larger than those presented here. Furthermore, the variation of the even−odd reaction rates presented here shows a 100−200 faster reaction for the even-numbered clusters and not only a factor of 2−3 as mentioned earlier.[21]
(38) Villano, S. M.; Huynh, L. K.; Carstensen, H.-H.; Dean, A. M. *J. Phys. Chem. A* **2011**, *115*, 13425.
(39) For the Al_{13}^- cluster, a ΔE^X value of −2.21 eV results, and therefore a smaller hindrance and a higher rate coefficient can be expected than for the $Ga_{13}^- + O_2$ reaction.
(40) This accelerating process between the $^3O_2$ molecule and the doublet $Ga_{10}^-/Ga_{12}^-/Ga_{14}^-$ clusters might be initiated by a preorientation of the magnetic species ($^3O_2/Ga_n^-$) with a short stabilization period of the loosely bonded magnetic contact pair, which is immediately followed by a strongly exoergic step; that is, these reactions proceed spontaneously. However, this hypothesis has to be

ruled out, because the energy of a hypothetic magnetic interaction is far below the thermal energy of the interacting species.
(41) In step **C**, only Al−O/Ga−O single bonds are formed like those in the gaseous reaction products Al−O−Al and Ga−O−Ga, respectively. For these linear molecules, bond energies of 5.35 eV (Al_2O) and 4.59 eV (Ga_2O) are known from experimental data.[2,3]
(42) Our simple model is also in line with the hindered $^3O_2$ reaction of Ag_{13}^- described recently:[11] The formation of neutral Ag_{13} (EA) (see Figure 3) requires the largest energy of all Ag_n^- clusters, that is, the lowest energy ($\Delta E^X = -0.5$ eV) is gained by the formation of the end-on $[O_2Ag_{13}]^-$ cluster, and consequently the electron transfer to an O_2^- species must overcome a high barrier, which is in line with an extremely slow reaction.
(43) (a) Yuan, Q. H.; Li, J.; Liu, Z.-F *Phys. Chem. Chem. Phys.* **2011**, *13*, 9871. (b) Han, Y.-K. *Phys. Chem. Chem. Phys.* **2012**, *14*, 6639. (c) Yuan, Q.; Liu, Z.-F. *Phys. Chem. Chem. Phys.* **2012**, *14*, 6641.
(44) Burgert, R.; Stokes, S. T.; Bowen, K. H.; Schnöckel, H. *J. Am. Chem. Soc.* **2006**, *128*, 7904.
(45) Weiß, K.; Schnöckel, H. *Int. J. Mass Spectrom.* **2002**, *214*, 383−395.
(46) Koch, K.; Schnöckel, H. *Z. Anorg. Allg. Chem.* **2007**, *633*, 873−878.
(47) Bach, S. B. H.; McElvany, S. W.; Wong, N. M.; Parent, D. C. *Chem. Phys. Lett.* **1993**, *209*, 57.
(48) (a) Becke, A. D. *Phys. Rev. A* **1999**, *38*, 3098. (b) Perdew, J. P. *Phys. Rev. B* **1986**, *33*, 8822.
(49) (a) Weigend, F.; Häser, M.; Patzelt, H.; Ahlrichs, R. *Chem. Phys. Lett.* **1998**, *294*, 143. (b) TURBOMOLE, V6.0, 2009, a development of University of Karlsruhe and Forschungszentrum Karlsruhe GmbH, 1989−2007, TURBOMOLE GmbH, since 2007; available from http://www.turbomole.com.
(50) Sierka, M. *Prog. Surf. Sci.* **2010**, *85*, 398.
(51) Kiran, B.; Kandalam, A. K.; Xu, J.; Ding, Y. H.; Sierka, M.; Bowen, K. H.; Schnöckel, H. *J. Chem. Phys.* **2012**, *137*, No. 134303.

Aluminum Zintl anion moieties within sodium aluminum clusters

Haopeng Wang,[1] Xinxing Zhang,[1] Yeon Jae Ko,[1] Andrej Grubisic,[1] Xiang Li,[1] Gerd Ganteför,[1] Hansgeorg Schnöckel,[2] Bryan W. Eichhorn,[3] Mal-Soon Lee,[4] P. Jena,[4] Anil K. Kandalam,[5,a)] Boggavarapu Kiran,[6,a)] and Kit H. Bowen[1,a)]
[1]*Department of Chemistry, Johns Hopkins University, Baltimore, Maryland 21218, USA*
[2]*Institute of Inorganic Chemistry, Karlsruhe Institute of Technology, 76128 Karlsruhe, Germany*
[3]*Department of Chemistry, University of Maryland at College Park, College Park, Maryland 20742, USA*
[4]*Department of Physics, Virginia Commonwealth University, Richmond, Virginia 23284, USA*
[5]*Department of Physics, West Chester University of Pennsylvania, West Chester, Pennsylvania 19383, USA*
[6]*Department of Chemistry, McNeese State University, Lake Charles, Louisiana 70609, USA*

(Received 26 November 2013; accepted 10 January 2014; published online 3 February 2014)

Through a synergetic combination of anion photoelectron spectroscopy and density functional theory based calculations, we have established that aluminum moieties within selected sodium-aluminum clusters are Zintl anions. Sodium–aluminum cluster anions, $Na_mAl_n^-$, were generated in a pulsed arc discharge source. After mass selection, their photoelectron spectra were measured by a magnetic bottle, electron energy analyzer. Calculations on a select sub-set of stoichiometries provided geometric structures and full charge analyses for both cluster anions and their neutral cluster counterparts, as well as photodetachment transition energies (stick spectra), and fragment molecular orbital based correlation diagrams. © *2014 AIP Publishing LLC*. [http://dx.doi.org/10.1063/1.4862989]

I. INTRODUCTION

Zintl phases are typically solid state, salt-like A_aX_x compounds formed from electropositive elements, A, and somewhat electronegative main-group elements, X.[1,2] Zintl phases are differentiated from traditional inter-metallics and semiconductors by their salt-like character, i.e., A^+ and X^-, and the presence of substantial X–X bonding.[3] The prototypical Zintl phase, NaTl, is best described as a $(Na^+)(Tl^-)$ salt containing a $[Tl^-]$ network, where the thallium anions form a diamond lattice with direct Tl–Tl bonds.[4]

Zintl anions are multiply negatively charged polyatomic aggregates of main group elements and are often associated with the solution-based chemistry of naked clusters, e.g., Sn_5^{2-}, Sb_7^{3-}, Pb_9^{4-}, and Bi_4^{2-}.[5] As in Zintl phases, Zintl anions are also characterized by X–X bonding. In addition, Zintl anions often have "pseudo-atom" equivalents as described by Klemm.[6] For example, As_8^{8-} and Sb_8^{8-} are isoelectronic and isostructural to the S_8 rings in elemental sulfur.[7,8] Most Zintl anions display multi-center, multi-electron bonding, and they can be described by the electronic counting principles developed for the boron hydrides.[5] For example, Ge_9^{4-} and Pb_{10}^{2-} have *nido* and *closo* deltahedral structures,[9,10] respectively, as predicted from Wade's rules of electron counting. While Zintl anions are most commonly associated with the heavier main group elements (≥period 4), clusters of the 3rd period are also known, e.g., $Si_9^{3-/4-}$ and P_7^{3-}.[5,11,12]

Although most studies on Zintl anions have been conducted in condensed phases, there is also a growing body of work in the gas phase. There, Zintl anions occur as Zintl moieties within larger clusters, the net charge state of which is determined by the number of complementary cationic moieties present. For example, Zintl anions in clusters were first implicated in photoionization mass spectral studies of III–V and IV–V intermetallic clusters.[13] Additionally, the presence of the Bi_3^{3-} Zintl anion was inferred from the observation of $(Na_4Bi_3)^+$ as a magic number species in mass spectra.[13,14] The occurrence of the Zintl anions: Sn_4^{4-}, Ga_4^{2-}, Sn_{12}^{2-}, and Pb_{12}^{2-} within the cluster anions: $(Na_4Sn_4)^-$, $(NaGa_4)^-$, $(KSn_{12})^-$, and $(KPb_{12})^-$, respectively, has also been shown through the combination of anion photoelectron experiments and theoretical calculations.[15–18] Furthermore, the existence of Zintl anions in several endohedral cage clusters, such as $[M@Pb_{12}]^{2-}$ and $M@(Sn_{12})^-$, where M is a transition metal atom, has also been inferred.[19–22]

Interestingly, Zintl anions of aluminum have not been prepared in solution or solid phases. Although LiAl is isoelectronic and isostructural with the prototypical Zintl phase, NaTl, early theoretical studies showed limited charge transfer between lithium and aluminum, thus deviating from the traditional definition of a Zintl phase.[23–25] More recent studies, however, have shown substantial Al–Al interactions in an $[Al^-]$ network structure with bonding motifs that conform to the Zintl-Klemm concept of a Zintl phase.[3,26] Nevertheless, with few exceptions,[3,27] most solid compounds of aluminum with alkali metals have not been classified as Zintl phases.

In the condensed phase, aluminum clusters are more commonly found in the form of low oxidation state "metalloid clusters" as described by Schnoeckel.[28] While there are significant similarities between Zintl ions and metalloid clusters, there are defining differences as well. For example, Zintl ions are anionic and have elemental oxidation states of less than zero. In contrast, the metalloids contain elements with oxidation states greater than zero but less than the maximum valence state of the element. Nevertheless, while standalone aluminum Zintl anions are not known in condensed

a)Authors to whom correspondence should be addressed. Electronic addresses: AKandalam@wcupa.edu, kiran@mcneese.edu, and kbowen@jhu.edu

phases, aluminum Zintl anion subunits can be found in some metalloid clusters. The recently reported $[Al(O\text{-}t\text{-}Bu)_3]_6Al_6^{8-}$ metalloid[29] contains an Al_6^{8-} core that has Zintl-like characteristics, suggesting that substituted or stabilized aluminum Zintl clusters may be viable.

Further insight into the viability of aluminum Zintl cluster moieties can be gleaned through studies of aluminum-containing, gas phase clusters. Several such systems have already been examined both experimentally and theoretically. The aluminum cluster anion, Al_{13}^- has received substantial attention because of its unusual stability, which derives both from its electronic (a 40 valence electron shell closing) and its geometric structure (an icosahedron).[30,31] The ionic character of KAl_{13}, i.e., K^+ and Al_{13}^-, was theoretically predicted[32–34] and later experimentally confirmed by both photoionization[35,36] of KAl_{13} and anion photoelectron experiments[37,38] of $(KAl_{13})^-$. Although Al_{13}^- is not multiply charged and differs in that way from traditional Zintl anions, KAl_{13} can be seen as a 14-atom, "diatomic," ionic "molecule" and as such, as the basic unit of a hypothetical aluminum-based "Zintl phase." Cluster anions, $(LiAl_n)^-$ (n = 3–13) and $(CuAl_n)^-$ (n = 2–15), were also investigated by anion photoelectron spectroscopy, where interest in the formation of salt-like structures motivated those studies.[39,40] To further investigate their bonding motifs, studies of all-metal aromaticity (and anti-aromaticity) were also carried out on $(MAl_4)^-$ (where M = Li, Na, and Cu), on $(MAl_6)^-$ (where M = Li, Na, K, Cu, and Au), and on $(Li_3Al_4)^-$ cluster anions[41–43] by using a combination of anion photoelectron spectroscopy and theoretical calculations. Several mixed sodium–aluminum clusters and their anions were also studied through theoretical calculations.[44] Recently, the isolated, multiply charged aluminum cluster anions, Al_n^{2-} and Al_n^{3-}, were formed by electron attachment to gas phase, singly charged aluminum cluster anions in a Penning trap; there, the smallest observed sizes were n = 38 and 103, respectively.[45] Taken together, these experimental and computational studies of doped or pure aluminum clusters in gas phase have laid the foundation for exploring multiply charged, aluminum Zintl cluster anion moieties within larger clusters.

One can imagine a salt-like lattice made up of aluminum cluster anions and counter cations. Calculations, however, suggest that such a lattice, when composed of K^+ and Al_{13}^- ions, would not be stable.[33] On the other hand, if such a lattice were composed, not of singly charged aluminum cluster anions, but instead of multiply charged, aluminum cluster anions, i.e., aluminum Zintl anions, with an appropriate number of complementary cations, then a substantially greater lattice stabilization energy could be achieved. Under those circumstances, the formation of a bulk ionic material, i.e., a cluster-assembled material might be feasible. A first step in exploring this possibility involves assessing whether aluminum Zintl anion moieties can exist within mixed alkali metal–aluminum clusters.

Here, we present a combined experimental and theoretical study aimed at determining whether multiply charged, aluminum Zintl anionic moieties are formed within sodium–aluminum clusters. On the experimental side, anion photoelectron spectroscopic measurements were carried out on size-selected, sodium-doped aluminum cluster anions, $Na_mAl_n^-$. The results of these experiments pertain both to the anionic clusters and to their corresponding neutral clusters. To better understand the various properties of mixed sodium/aluminum clusters, calculations based on density functional theory (DFT) were also carried out both on the cluster anions and their neutral cluster counterparts. In addition to calculating photodetachment (photoelectron) transition energies for the cluster anions and geometric structures for both the cluster anions and their neutral counterparts, we also conducted full charge analyses through Natural Population Analysis (NPA), for both the cluster anions and their corresponding neutral clusters. Calculated photodetachment transition energies were compared with measured transitions in the photoelectron spectra. Geometric structures revealed the sub-structure of the aluminum cluster moieties and how the sodium atoms were arranged around them. Natural population analyses illuminated the extent of Zintl anion character in the aluminum moieties within these clusters. As such, NPA was our primary tool for identifying Zintl anion character in specific aluminum cluster moieties. Among the many sodium–aluminum cluster anions that we generated and studied by photoelectron spectroscopy, five stoichiometries and their neutral counterparts were selected to undergo the detailed theoretical analysis described above. These were $Na_2Al_6^-$, $Na_4Al_5^-$, $Na_5Al_5^-$, $Na_3Al_{12}^-$, and $Na_4Al_{12}^-$ as well as their neutral counterparts, Na_2Al_6, Na_4Al_5, Na_5Al_5, Na_3Al_{12}, and Na_4Al_{12}, respectively. These stoichiometries were chosen in part because they are all closed shell species[46] in either their anion or their neutral charge states. As closed shells, they would be expected to exhibit enhanced stability. The degree to which particular cluster stoichiometries conformed to the expectations of the shell model was explored through fragment molecular orbital (FMO) calculations and their resultant correlation diagrams.[47]

II. METHODS

A. Experimental

Anion photoelectron spectroscopy is conducted by crossing a mass-selected beam of negative ions with a fixed-frequency photon beam and energy-analyzing the resultant photodetached electrons. It is governed by the energy-conserving relationship, $h\nu = EBE + EKE$, where $h\nu$ is the photon energy, EBE is the electron binding (transition) energy, and EKE is the electron kinetic energy. Briefly, our apparatus, which has been described previously,[48] consists of a pulsed arc cluster ionization source (PACIS),[49] a time-of flight mass spectrometer for mass analysis and mass selection, a Nd:YAG laser operated in these experiments at its third harmonic wavelength (355 nm, 3.49 eV/photon) for photodetachment, and a magnetic bottle, electron energy analyzer with a resolution of 30 meV at EKE = 1 eV. The photoelectron spectra were calibrated against the well-known photoelectron spectrum of Cu^-.[50]

In our pulsed arc cluster ionization source, a discharge is triggered between an anode and a grounded, conductive, sample cathode, while helium gas from a pulsed valve

is fed through the discharge region. In the present study, the sample cathode consists of an aluminum rod, with a cup-like depression on top, into which a mixture of aluminum powder and particles of sodium metal had been pressed into a disk. The sample material is vaporized by the discharge, cooled by the helium jet, and forms cluster anions as it travels down a 20 cm tube into high vacuum. The resulting cluster anions are then extracted, mass analyzed, and mass selected prior to being irradiated by photons.

B. Computational

Density functional theory based electronic structure calculations on Na_2Al_6, Na_4Al_5, Na_5Al_5, Na_3Al_{12}, and Na_4Al_{12} clusters and their anions were carried out using the Gaussian03 program.[51] The B3LYP functional form and the 6-311+G* basis set were used for all the calculations. The reliability of the theoretical method and the basis set used in this study had been established in a previous study on MAl_6^- (M = Li, Na, K, Cu, and Au) bi-metallic clusters.[42] During the geometry optimizations, the convergence criterion for energy was set to 10^{-9} hartree, while the gradient was converged to 10^{-4} hartree/Å. The vibrational frequencies of the reported isomers were calculated and found to be positive, indicating that these isomers are all minima on the potential energy surface. NPA, as implemented in the Gaussian03 code, were also carried out to determine the charge distributions in these clusters. The FMO of these five closed shell clusters were calculated at PW91/TZ2P using Amsterdam Density Functional Program.[52–54]

III. RESULTS AND DISCUSSION

The photoelectron spectra of all the $Na_mAl_n^-$ cluster anions measured in this study are presented in Figure 1. They were recorded using third harmonic (355 nm, 3.49 eV) photons from a Nd:YAG laser. The electron binding energies (EBE) of the peaks in each spectrum provide the photodetachment transition energies from the ground electronic state of the cluster anion to the ground and excited electronic states of the cluster anion's neutral counterpart. The EBE value near the onset (threshold) of the lowest EBE peak in a given photoelectron spectrum was taken as an estimate of the adiabatic electron affinity, EA, of the anion's neutral counterpart. The EBE value at the intensity maximum in the lowest EBE peak in the spectrum is the vertical detachment energy, VDE, which reflects the maximum Franck-Condon overlap between the wave functions of the anion's electronic ground state and the neutral's electronic ground state at the geometry of the anion.

Note that when neutral Na_mAl_n clusters exhibit closed electronic shell, with magic numbers of valence electrons, e.g., … 8, 18, 20, 34, 40, 58 …, the onset EBE values (estimated EA values) in their anions' photoelectron spectra tend to be smaller than those of their similar size neighbors. Additionally, the spacings between the lowest EBE and the next higher EBE peaks (the neutral clusters' HOMO-LUMO gaps) tend to be larger than those of their neighbors. On the other hand, when $Na_mAl_n^-$ cluster anions have closed electronic shell with magic number of valence electrons, their onset EBE values are higher than those of their similar size neighbors. In Figure 1, neutral closed shell Na_mAl_n clusters are marked with "**n**," while "**a**" closed shell $Na_mAl_n^-$ anions.

As described above, we have selected five of these $Na_mAl_n^-$ cluster anions and their neutral cluster counterparts for detailed computational scrutiny. These cluster anion/neutral cluster systems are: $Na_2Al_6^-/Na_2Al_6$, $Na_4Al_5^-/Na_4Al_5$, $Na_5Al_5^-/Na_5Al_5$, $Na_3Al_{12}^-/Na_3Al_{12}$, and $Na_4Al_{12}^-/Na_4Al_{12}$. Our calculations provided both the vertical detachment energy and the adiabatic detachment energy, ADE, for each of these anions, where ADE is the energy difference between the ground state geometry of the anionic cluster and the structurally similar/identical isomer (nearest local minimum) of its neutral counterpart. When the neutral and its anion have similar geometries, ADE = EA. Since our calculations show this structural similarity to be the case in the systems studied here, with the possible exception of the $Na_4Al_{12}^-/Na_4Al_{12}$ pair, the computed ADE value can be compared with the experimental EBE value at the spectral threshold, i.e., its estimated EA value. Table I presents both calculated and measured values of VDE and of ADE/EA.

Below, the five designated cluster anion/neutral cluster systems are presented and discussed in turn. In each case, we first present the calculated geometric structures of the lowest energy isomers of the cluster anion and its neutral cluster counterpart along with the natural population analysis for each structure. The extent of Zintl anion character in the aluminum moieties is then discussed in terms of their charge analyses. Next, we present the cluster anion's photoelectron spectrum along with its stick spectrum, the latter reflecting the calculated photodetachment transitions from the cluster anions' lowest energy isomers. Finally, we provide FMO correlation diagrams that support the closed electronic shell character of that particular cluster anion or its neutral counterpart.

A. $Na_2Al_6^-/Na_2Al_6$

Figure 2 presents the calculated structures of the three lowest energy isomers of $Na_2Al_6^-$ and Na_2Al_6 clusters. The most stable isomers, for both the anion and the neutral, are found to be Al_6 prisms with their two sodium atoms capping the faces of the two adjacent four-member rings (see structures, **1** and **4**). The structures of the second (**2** and **5**) and third (**3** and **6**) lowest energy isomers, which are 0.12 (0.10) eV and 0.16 (0.14) eV higher in energy than the corresponding lowest energy anion (neutral), are made up of Al_6 octahedra differing only in the positions of their sodium atoms over the surface of the cluster. Note that the Al_6 units (prism and octahedra) within the cluster anions are distorted relative to those within their corresponding neutral clusters. This is the result of the extra electron interacting with the Al_6 unit in each anionic isomer.

Since alkali metal atoms are significantly more electropositive than aluminum atoms, one might expect considerable charge transfer, formally 1*e*, from each sodium atom to the aluminum cluster moiety, leading to $(Na^+)_2(Al_6^{2-})$ in the

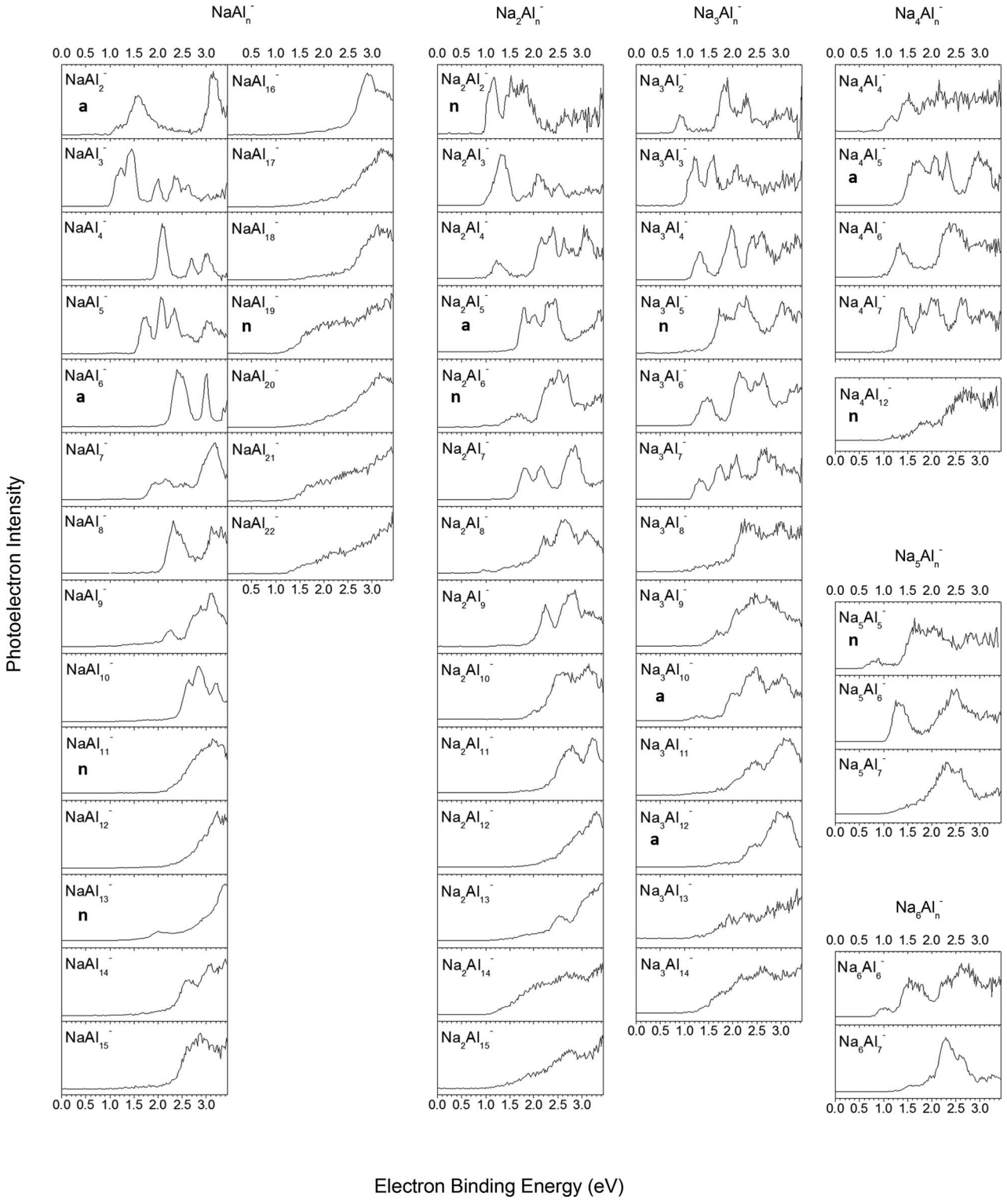

FIG. 1. Photoelectron spectra of $Na_mAl_n^-$ cluster anions, (m = 1, n = 2–22; m = 2, n = 2–15; m = 3, n = 2–14; m = 4, n = 4–7 and 12; m = 5, n = 5–7; m = 6, n = 6–7). Species with closed shell neutrals are marked by "**n**," and those with closed shell anions are marked by "**a**." Note that the valence electrons for these closed shell clusters, based on the jellium model, are 8, 18, 20, 34, 40, and 58.

case of the Na_2Al_6 neutral cluster. However, our NPA charge distribution analysis shows that a smaller amount of negative charge is actually transferred. In isomer **4**, both sodium atoms together donate $-1.54e$, instead of $-2.0e$, to Al_6 prism (see Figure 2). With a charge of $-1.54e$, we classify the Al_6 moiety as an incipient Zintl anion. In the case of the $Na_2Al_6^-$ cluster anion, where the net charge on the entire cluster is, by definition, $-1e$ and where the Al_6 moiety holds the lion's share of the negative charge ($-2.32e$ in isomer **1**), the two sodium atoms together contribute less negative charge to the aluminum moiety than they did in the case of the Na_2Al_6 neutral cluster. Interestingly, among the isomers of $Na_2Al_6^-$, as

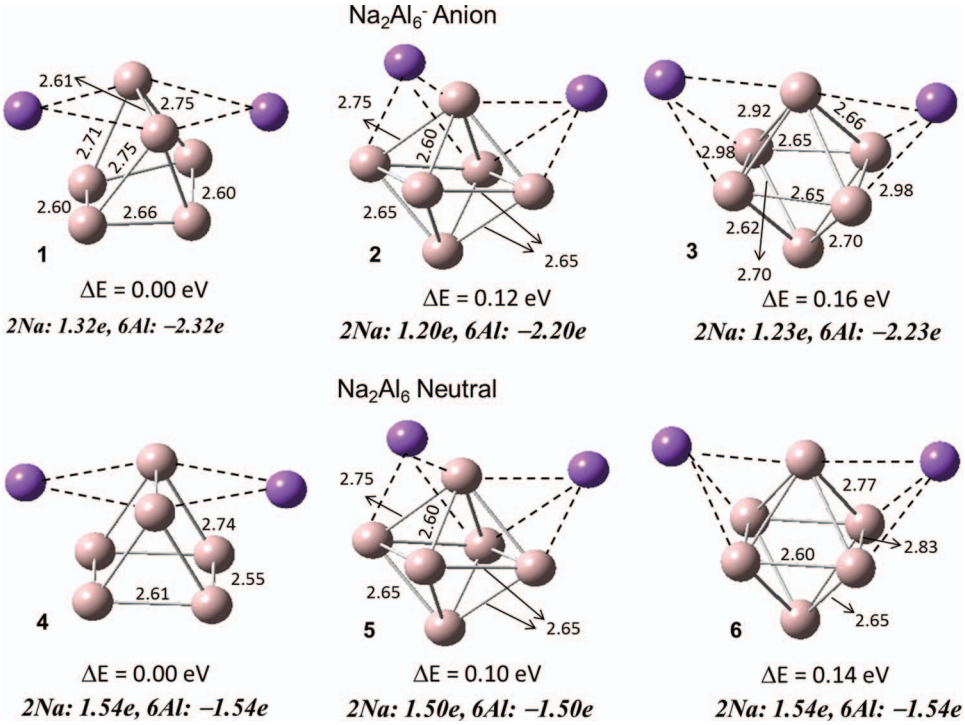

FIG. 2. The three lowest energy isomers of the $Na_2Al_6^-$ cluster anion and the Na_2Al_6 neutral cluster along with their relative energies, ΔE (eV). Isomers **1**–**3** correspond to the $Na_2Al_6^-$ anion, while **4**–**6** correspond to the lowest energy isomers of neutral Na_2Al_6. The gray spheres represent aluminum atoms and the purple spheres represent sodium atoms. All the bond lengths are given in Å. The calculated Natural Population Analysis (NPA) charges are given in italics below each isomer.

well as among those of Na_2Al_6, the extent of charge transfer to their respective Al_6 moieties is similar, even though the geometries of the Al_6 moieties vary from isomer to isomer.

Figure 3 presents the photoelectron spectrum of the $Na_2Al_6^-$ cluster anion. The first two photodetachment transitions have been calculated for each of the three lowest energy isomers of the $Na_2Al_6^-$ anion (**1**–**3**), and these are presented as stick spectra in Figure 3 (solid, dashed, and dotted sticks are for transitions from **1**, **2**, and **3**, respectively). Focusing on the lower energy transition, the calculated values of ADE and VDE for isomers **1** (1.20 eV and 1.63 eV), **2** (1.18 eV and 1.47 eV), and **3** (1.14 eV and 1.41 eV) compare well with the experimentally determined EA and VDE values of 1.20 and 1.66 eV, respectively (see Table I). Based on the calculated and measured values, it appears that all three anionic isomers may be present in the beam. Since neutral Na_2Al_6 is a closed shell species (see below), the spacing between the first two transitions in the photoelectron spectrum provides its HOMO-LUMO gap. At ∼0.7 eV, this gap reflects the stability of neutral Na_2Al_6. Generally, the computational and experimental results are in good agreement.

Confirmation that the Na_2Al_6 neutral cluster, with its 20 valence electrons, exhibits electronic shell closure behavior is provided by its calculated FMO correlation diagram (see Figure 4). It shows that the levels group themselves into the

TABLE I. Experimental EA and theoretical ADE values of Na_2Al_6, Na_4Al_5, Na_5Al_5, Na_3Al_{12}, and Na_4Al_{12} neutral clusters and VDE values of $Na_2Al_6^-$, $Na_4Al_5^-$, $Na_5Al_5^-$, $Na_3Al_{12}^-$, and $Na_4Al_{12}^-$ cluster anions. All values are in eV. The calculated values for all low energy isomers are listed; the first listed value corresponds to the lowest energy isomer.

	ADE	EA	VDE	
Cluster	Theo.	Expt.	Theo.	Expt.
Na_2Al_6	1.20, 1.18, 1.14	1.20	1.63, 1.47, 1.41	1.66
Na_4Al_5	1.41, 1.68	1.44	1.52, 1.92	1.55
Na_5Al_5	0.64, 0.92	0.57	0.89, 1.02	0.87
Na_3Al_{12}	2.04	2.08	2.31	2.43
Na_4Al_{12}	1.21	1.45	1.88	1.89

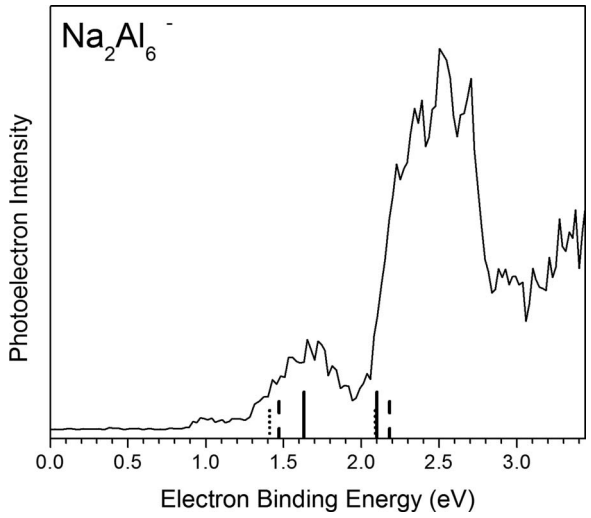

FIG. 3. Photoelectron spectrum of the $Na_2Al_6^-$ cluster anion. The overlaid stick spectra indicate the calculated first two transitions from the $Na_2Al_6^-$ anion to its corresponding neutral cluster. (Solid sticks: isomer **1**; dashed sticks: isomer **2**; dotted sticks: isomer **3**.)

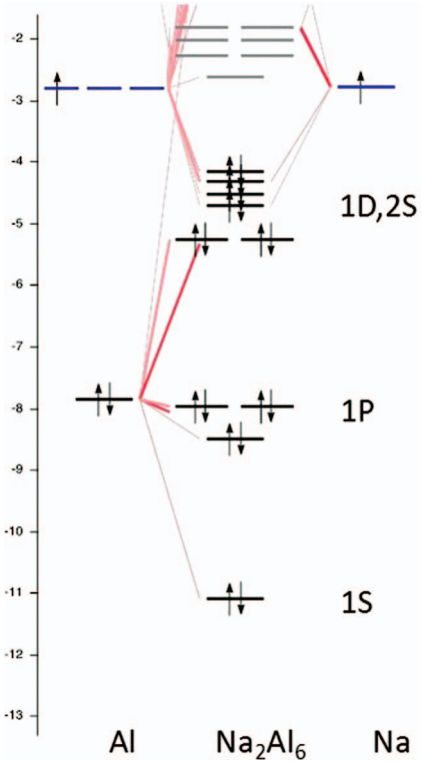

FIG. 4. The fragment molecular orbitals (FMO) analysis for the Na_2Al_6 neutral cluster.

1S, 1P, 1D/2S pattern expected under the jellium-like shell model[46] for free electron metals such as sodium and aluminum.

B. $Na_4Al_5^-/Na_4Al_5$

Figure 5 presents the computed structures of the two lowest energy isomers of $Na_4Al_5^-$ and Na_4Al_5 clusters. The lowest energy isomers of the $Na_4Al_5^-$ cluster anion, **7**, and the neutral Na_4Al_5 cluster, **9**, both adopt distorted octahedral-like structures, these being formed by an Al_5 square pyramid and a sodium atom occupying one of the vertices. The remaining three sodium atoms cap triangular faces. The second lowest energy isomers of the cluster anion, **8**, and the neutral cluster, **10**, are also both made up of Al_5 square pyramids. However, in each of these cases, all four of their sodium atoms bind to the base of their Al_5 square pyramids. Also, notice that while the energy difference between anion's two isomer structures is quite small (0.07 eV), the energy difference is significantly larger (0.35 eV) between the neutral's two isomer structures.

As in $Na_2Al_6^-$, the charge distributions in the isomers of the $Na_4Al_5^-$ cluster anion show that the majority of their excess electron resides on their aluminum moieties. Unlike $Na_2Al_6^-$, however, the net charge transfer in $Na_4Al_5^-$ to its Al_5 moiety differs considerably from isomer to isomer, with Al_5 in **7** receiving -3.27 *e* but with Al_5 in **8** getting only -2.51 *e*. The difference may be due to the relatively symmetric location of the four sodium atoms around the Al_5 moiety in isomer **7**, compared with the asymmetric location of sodium atoms around this moiety in isomer **8**. In the case of the neutral Na_4Al_5 cluster, the charge distributions in isomers, **9** and

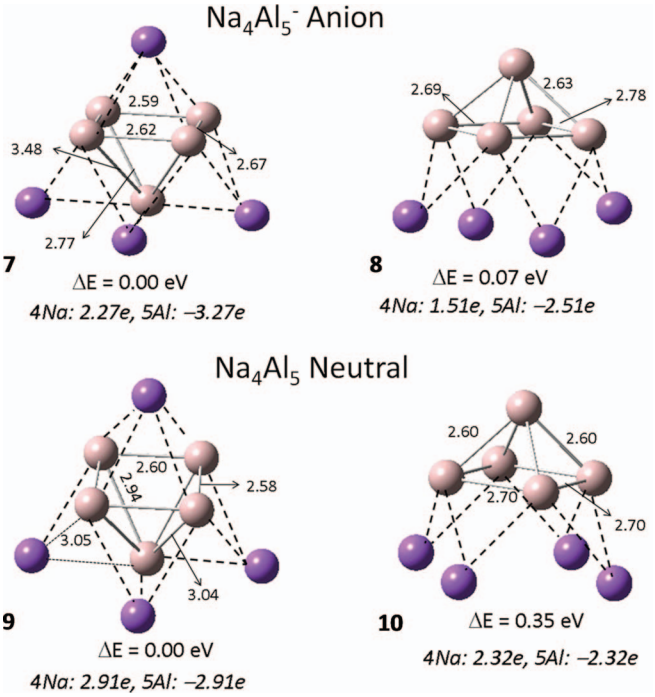

FIG. 5. The two lowest energy isomers of the $Na_4Al_5^-$ cluster anion and the Na_4Al_5 neutral cluster along with their relative energies, ΔE (eV). Isomers **7** and **8** correspond to the $Na_4Al_5^-$ cluster anion, while **9** and **10** correspond to the lowest energy isomers of the neutral Na_4Al_5 cluster. The gray spheres represent aluminum atoms and the purple spheres represent sodium atoms. All the bond lengths are given in Å. The calculated Natural Population Analysis (NPA) charges are given in italics below each isomer.

10, show that their Al_5 moieties possess net negative charges of about -2.9 *e* and -2.3 *e*, respectively, this difference as well being influenced by the relative positions of the sodium atoms around the Al_5 moieties. These Al_5 aluminum moieties are clearly Zintl anions. A trend is emerging whereby multiply charged aluminum cluster moieties, i.e., aluminum Zintl anions, are more likely to form in sodium–aluminum clusters when several sodium atoms are available.

Figure 6 presents the photoelectron spectrum of the $Na_4Al_5^-$ cluster anion. The first few sets of photodetachment transitions have been calculated for each of the two lowest energy isomers of the $Na_4Al_5^-$ cluster anion (**7** and **8**), and these are presented as stick spectra in Figure 6 (solid and dashed sticks are for transitions from **7** and **8**, respectively). We have calculated ADE and VDE values for the lower energy transition in the cases of both isomer **7** and isomer **8** (see Table I). The VDE of **7** is 1.52 eV, and it matches well with the experimental value of 1.55 eV. On the other hand, the VDE of **8**, which is 1.92 eV, is significantly higher in energy than the observed value. The ADE values follow similar trends. The ADE of **7** is 1.41 eV, and this is close to the estimated value of 1.44 eV, whereas the ADE of **8** is 1.68 eV. Thus, it is likely that only isomer **7** is present in the cluster anion beam. Comparison of stick spectra for the two isomers with the experimental spectrum (see Figure 6) leads to the same conclusion.

In this system, the 20 valence electron, closed shell cluster is the $Na_4Al_5^-$ cluster anion. Figure 7 presents the calculated FMO correlation diagram for the $Na_4Al_5^-$ cluster anion. In a 20 valence electron cluster that obeys the jellium-like

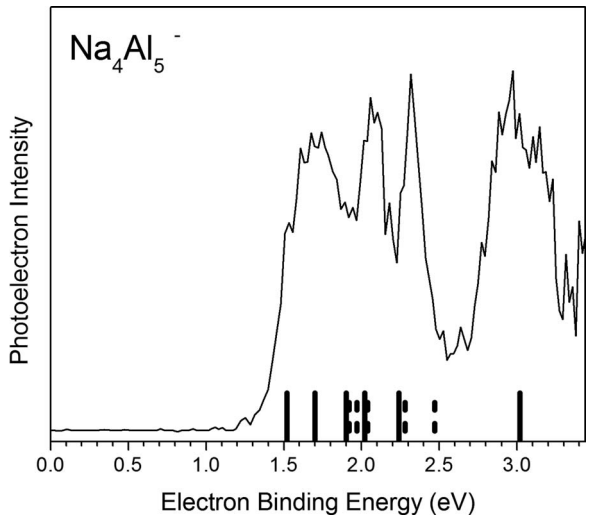

FIG. 6. Photoelectron spectrum of the $Na_4Al_5^-$ cluster anion. The overlaid stick spectra indicate the calculated low energy transitions from the $Na_4Al_5^-$ anion to its corresponding neutral cluster. (Solid sticks: isomer **7**; dashed sticks: isomer **8**.)

model, one would expect the 1*S* 1*P* 1*D* and 2*S* levels to be filled. It is evident from Figure 7 that the expected 20 valence electron, shell-closing is observed. The resulting MO energy levels form three distinct blocks, with the lowest two blocks corresponding to 1*S* and 1*P*, and with the frontier block encompassing 1*D* and 2*S*. Because the $Na_4Al_5^-$ cluster anion is a closed shell species, it would be expected to exhibit high

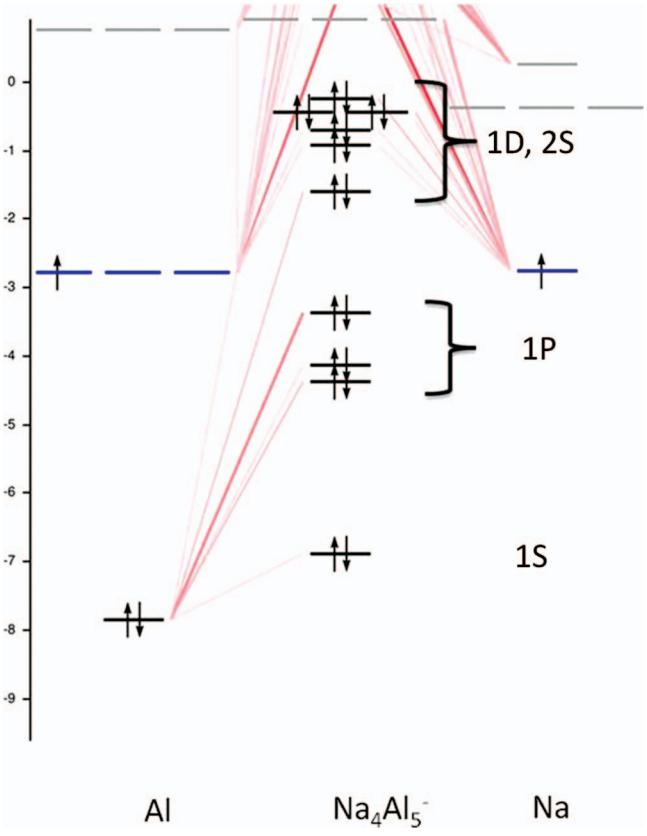

FIG. 7. The fragment molecular orbitals (FMO) analysis for the $Na_4Al_5^-$ cluster anion.

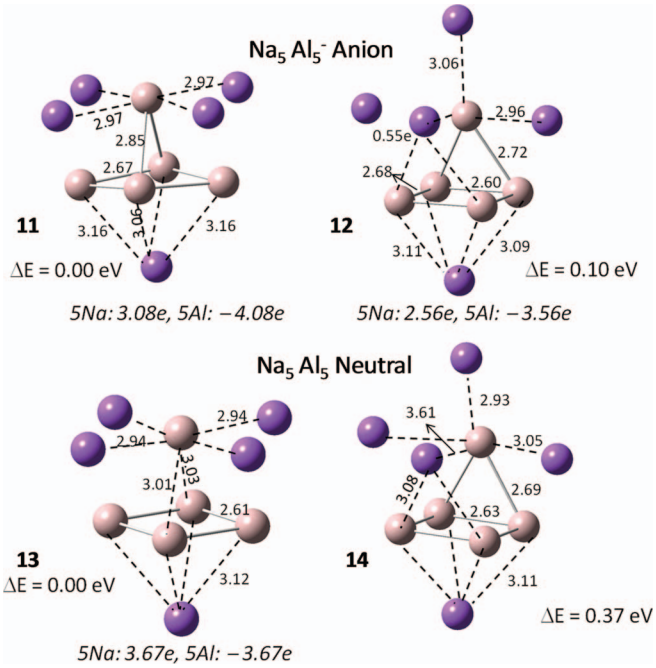

FIG. 8. The two lowest energy isomers of the $Na_5Al_5^-$ cluster anion and the Na_5Al_5 neutral cluster along with their relative energies, ΔE (eV). Isomers **11** and **12** correspond to the $Na_5Al_5^-$ anion, while **13** and **14** correspond to the lowest energy isomers of neutral Na_5Al_5. The gray spheres represent aluminum atoms and the purple spheres represent sodium atoms. All the bond lengths are given in Å. The calculated Natural Population Analysis (NPA) charges are given in italics below each isomer.

electron detachment energy. The fact that it does not may be due to excess negative charge accumulation on the Al_5 moiety, causing a destabilization of the frontier orbitals and thereby reducing the shell-closing effects in this system.

C. $Na_5Al_5^-/Na_5Al_5$

The calculated structures of the lowest energy isomers of the $Na_5Al_5^-$ cluster anion (**11** and **12**) and of the Na_5Al_5 neutral cluster (**13** and **14**) are presented in Figure 8. As in the $Na_4Al_5^-$ cluster anion and the Na_4Al_5 neutral cluster, the $NaAl_5$ sub-units in the lowest energy isomers of the $Na_5Al_5^-$ cluster anion (**11**) and the Na_5Al_5 neutral cluster (**13**) also adopt distorted octahedral geometries, with the remaining sodium atoms occupying various positions around this central core. Not surprisingly, the relative energies of the isomers of $Na_5Al_5^-$ and Na_5Al_5 are also similar to those of $Na_4Al_5^-$ and Na_4Al_5.

The $-3.67e$ charge on the Al_5 moiety of the Na_5Al_5 neutral cluster (structure **13**) shows that it is a Zintl anion. It is interesting to compare isoelectronic sodium/aluminum clusters, such as the $Na_4Al_5^-$ cluster anion and the Na_5Al_5 neutral cluster, where the additional sodium atom in Na_5Al_5 provides the extra negative charge (extra electron) in $Na_4Al_5^-$. In the $Na_4Al_5^-$ cluster anion (structure **7**), the net charge on the Al_5 moiety is $-3.27e$, whereas in the similarly structured Na_5Al_5 neutral cluster (structure **13**), it is $-3.67e$. The actual negative charges on the Al_5 moieties are comparable, regardless of the net charge state. Also, the net charge on the Al_5 moiety of the $Na_5Al_5^-$ cluster anion is $-4.08e$. The Al_5 moiety has

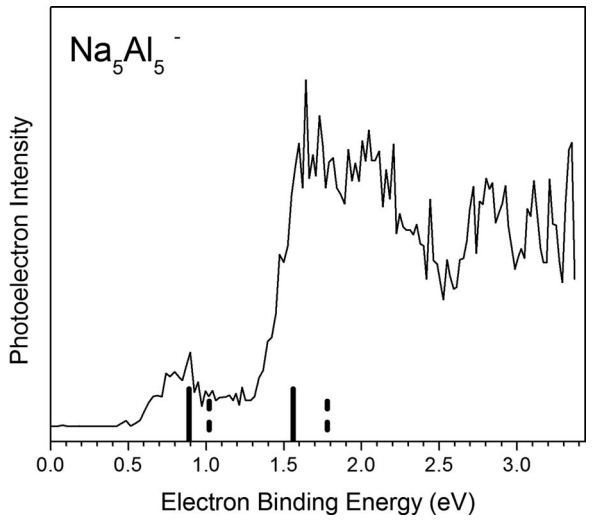

FIG. 9. Photoelectron spectrum of the $Na_5Al_5^-$ cluster anion. The overlaid stick spectra indicate the calculated first two transitions from the $Na_5Al_5^-$ cluster anion to its corresponding neutral cluster. (Solid sticks: isomer **11**; dashed sticks: isomer **12**.)

a propensity for forming Zintl anions when paired with five sodium atoms.

The photoelectron spectrum of the $Na_5Al_5^-$ cluster anion is presented in Figure 9. The first two photodetachment transitions have been calculated for each of the two lowest energy isomers of the $Na_5Al_5^-$ anion (**11** and **12**), and these are presented as stick spectra in Figure 9 (solid and dashed sticks are for transitions from **11** and **12**, respectively). We have calculated ADE and VDE values for the lower energy transition in the cases of both isomer **11** and isomer **12** (see Table I). The calculated VDE of **11** is 0.89 eV, and it compares well with the experimental value of 0.87 eV. On the other hand, the VDE of **12**, which is 1.02 eV, is significantly higher in energy than the observed value. The ADE values follow similar trends. The calculated ADE of **11** is 0.64 eV, and this is close to the estimated EA value of 0.57 eV, whereas the ADE of **12** is 0.92 eV. This suggests that only isomer **11** may be present in the cluster anion beam, although the stick spectra are consistent with both being present. Since the neutral Na_5Al_5 cluster is a 20 valence electron, closed shell species (see below), the spacing between the first two transitions in the photoelectron spectrum of the $Na_5Al_5^-$ cluster anion reflects the HOMO-LUMO gap of the neutral Na_5Al_5 cluster. At ~0.7 eV, this gap reflects the stability of the closed shell Na_5Al_5 neutral cluster, just as it did in the case of neutral Na_2Al_6. The computational results show good agreement with the experimental photoelectron spectrum.

With 20 valence electrons, the Na_5Al_5 neutral cluster meets the condition for electronic shell closure. Figure 10 presents the calculated FMO correlation diagram for the Na_5Al_5 neutral cluster, where it exhibits three distinct blocks of MO energy levels, reflecting the 1S, 1P, 1D/2S pattern expected under the jellium-like model for a closed shell species. Not surprisingly, the isoelectronic species, $Na_4Al_5^-$ and Na_5Al_5 yield very similar, yet not identical FMO correlation diagrams (see Figures 7 and 10, respectively).

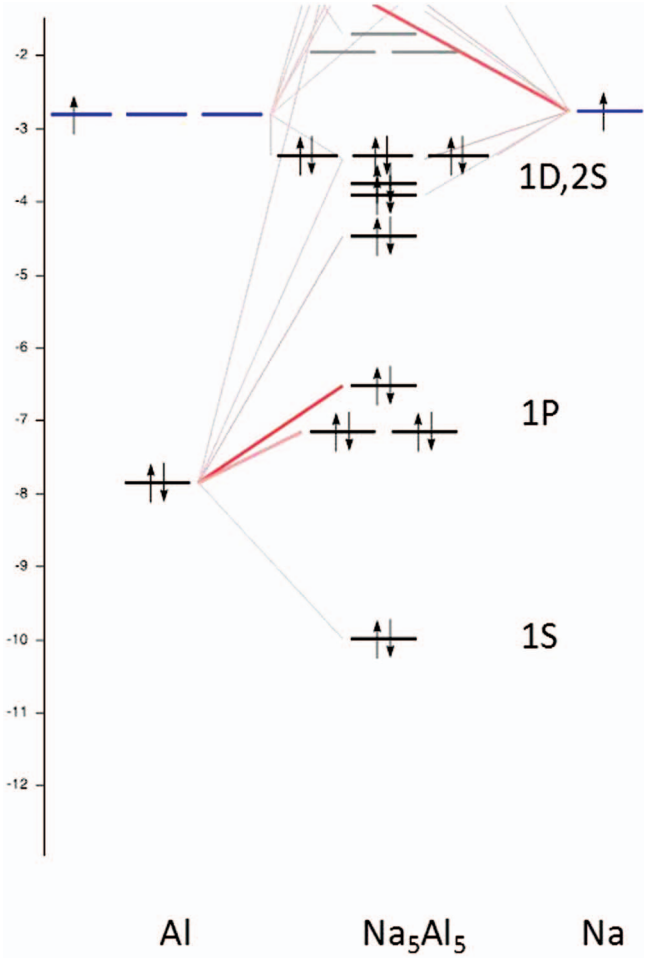

FIG. 10. The fragment molecular orbitals (FMO) analysis for the Na_5Al_5 neutral cluster.

D. $Na_3Al_{12}^-/Na_3Al_{12}$

Figure 11 presents the lowest energy structures of the $Na_3Al_{12}^-$ anion (**15**) and the Na_3Al_{12} neutral (**16**). Both of these exhibit rhombohedral-like structures, with an aluminum atom at the center, a sodium atom at one of the apexes, and the remaining two sodium atoms capping the two adjacent four-member rings. Other anion and neutral isomers of these clusters (not shown), where two sodium atoms cap two alternate four membered rings are also found to have energies which are close to those of the lowest energy structures. Substantial charge transfer to their Al_{12} moieties was found in both the $Na_3Al_{12}^-$ cluster anion ($-2.90e$) and in the Na_3Al_{12} neutral cluster ($-2.17e$). The Al_{12} moiety within the Na_3Al_{12} neutral cluster is a Zintl anion.

Figure 12 presents the photoelectron spectrum of the $Na_3Al_{12}^-$ cluster anion. The first photodetachment transition has been calculated for the lowest energy isomer of the $Na_3Al_{12}^-$ anion (**15**), and this is presented as a stick spectrum in Figure 12. We have calculated ADE and VDE values for this transition in the case of this isomer (see Table I). The calculated VDE is 2.31 eV, and it compares well with the experimental value of 2.43 eV. The calculated ADE is 2.04 eV, and this is close to the estimated EA value of 2.08 eV. The computational results show good agreement with the spectrum.

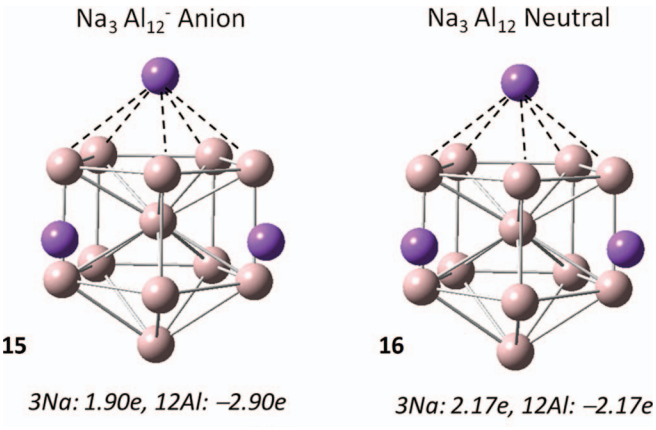

FIG. 11. The lowest energy isomers of the $Na_3Al_{12}^-$ cluster anion (**15**) and the Na_3Al_{12} neutral cluster (**16**). The gray spheres represent aluminum atoms and the purple spheres represent sodium atoms. The calculated Natural Population Analysis (NPA) charges are given in italics below each isomer.

The $Na_3Al_{12}^-$ cluster anion possesses 40 valence electrons, where 40, like 20, is an electronic shell closing, magic number. Figure 13 presents the calculated FMO correlation diagram for the $Na_3Al_{12}^-$ cluster anion. For 40 electrons, the expected filling order of the shells is 1*S* 1*P* 1*D* 2*S* 1*F* 2*P*. As shown in Figure 13, the MO energy levels fall into four distinct blocks, corresponding to (1*S*), (1*P*), (1*D*, 2*S*), and (1*F*, 2*P*), thus supporting the expectation that the $Na_3Al_{12}^-$ cluster anion conforms to a 40 valence electron shell closure. Furthermore, because $Na_3Al_{12}^-$ is a closed shell species, it is expected to exhibit a relatively high electron affinity, and with ADE and estimated EA values of 2.04 eV and 2.08 eV, respectively, it does.

E. $Na_4Al_{12}^-/Na_4Al_{12}$

As shown in Figure 14, the $Na_4Al_{12}^-$ cluster anion adopts a capped icosahedral-like structure, with its missing vertices occupied by sodium atoms (see structure **17**), while the Na_4Al_{12} neutral cluster exhibits a rhombohedral-like structure (see structure **18**). The structure of the latter is, in fact, quite similar to that of its isoelectronic counterpart, the $Na_3Al_{12}^-$ cluster anion, cf. structure **15**.

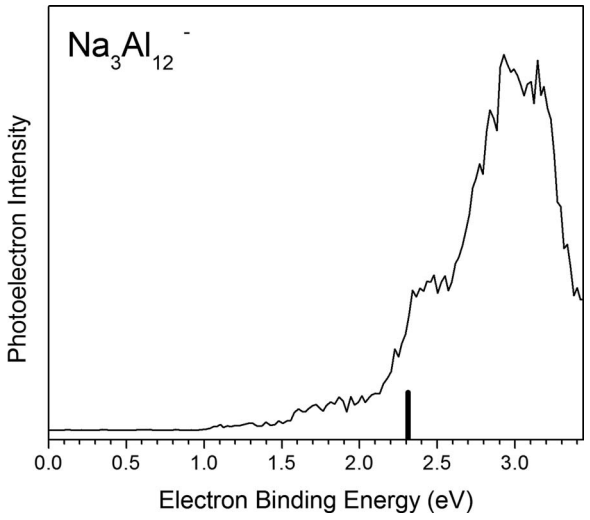

FIG. 12. Photoelectron spectrum of the $Na_3Al_{12}^-$ cluster anion. The overlaid stick spectra indicate the calculated transitions from the ground state of the $Na_3Al_{12}^-$ cluster anion to the ground state of the Na_3Al_{12} neutral cluster.

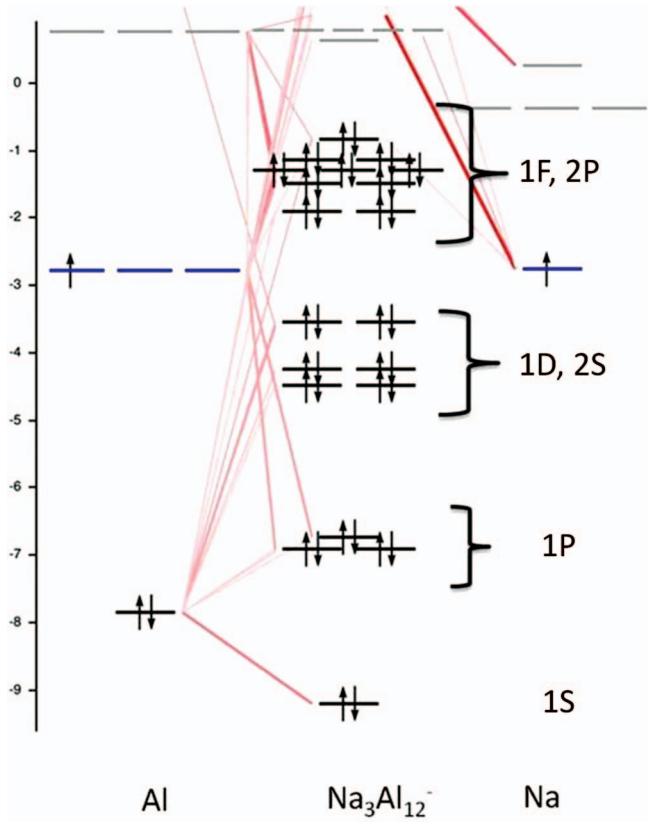

FIG. 13. The fragment molecular orbitals (FMO) analysis for the $Na_3Al_{12}^-$ cluster anion.

Charge analyses of the $Na_4Al_{12}^-$ cluster anion and the Na_4Al_{12} neutral cluster reveal net charges on their Al_{12} moieties of $-4.14e$ and $-3.43e$, respectively. Comparing the isoelectronic species, Na_4Al_{12} and $Na_3Al_{12}^-$, shows that the charges on their Al_{12} moieties are $-3.43e$ and $-2.90e$, respectively. It is interesting that the Al_{12} moiety within the Na_4Al_{12} neutral cluster possesses more negative charge than

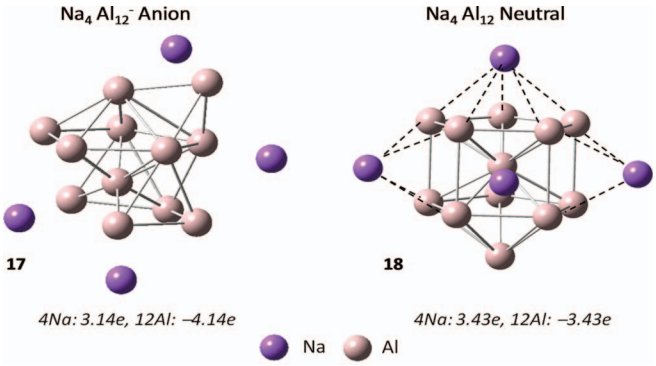

FIG. 14. The lowest energy isomers of the $Na_4Al_{12}^-$ cluster anion (**17**) and the Na_4Al_{12} neutral cluster (**18**). The gray spheres represent aluminum atoms and the purple spheres represent sodium atoms. The calculated Natural Population Analysis (NPA) charges are given in italics below each isomer.

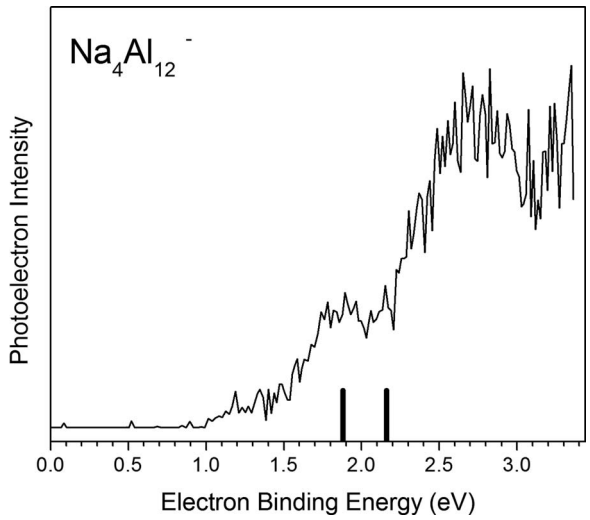

FIG. 15. Photoelectron spectrum of the $Na_4Al_{12}^-$ cluster anion. The overlaid stick spectra indicate the calculated transitions from the ground state of the $Na_4Al_{12}^-$ cluster anion to the ground and first excited states of the Na_4Al-_{12} neutral cluster.

the Al_{12} moiety within the $Na_3Al_{12}^-$ cluster anion. The Al_{12} moiety within the Na_4Al_{12} neutral cluster is a robust Zintl anion.

Figure 15 presents the photoelectron spectrum of $Na_4Al_{12}^-$ cluster anion. The first two photodetachment transitions have been calculated for the lowest energy isomer of the $Na_4Al_{12}^-$ anion, **17**, and these are presented as a stick spectrum in Figure 15. We have also calculated ADE and VDE values for the lower energy transition in the case of this isomer (see Table I). The calculated VDE is 1.88 eV, and it compares well with the experimental value of 1.89 eV. The calculated ADE is 1.21 eV, and this is in reasonable agreement with the estimated EA value of 1.45 eV. Since the Na_4Al_{12} neutral cluster is a 40 valence electron, closed shell species (see below), the spacing between the first two transitions in the photoelectron spectrum of the $Na_4Al_{12}^-$ cluster anion reflects the HOMO-LUMO gap of the neutral Na_4Al_{12} cluster. This computed HOMO-LUMO gap is ~0.3 eV. It reflects the enhanced stability of the closed shell Na_4Al_{12} neutral cluster, just as earlier discussed HOMO-LUMO gaps reflected the enhanced stabilities of the Na_2Al_6 and Na_5Al_5 neutral clusters. While the signal-to-noise ratio of the $Na_4Al_{12}^-$ cluster anion photoelectron spectrum leads to some degree of uncertainty, the calculated gap and observed spacing are broadly consistent.

The Na_4Al_{12} neutral cluster possesses 40 valence electrons, where 40 is a magic number. Figure 16 presents the calculated FMO correlation diagram for the Na_4Al_{12} neutral cluster. For 40 electrons, the expected filling order is 1*S* 1*P* 1*D* 2*S* 1*F* 2*P*. As shown in Figure 16, the MO energy levels fall into four distinct blocks, corresponding to (1*S*), (1*P*), (1*D*, 2*S*), and (1*F*, 2*P*), thus supporting the expectation that the Na_4Al_{12} neutral cluster is a 40 valence electron closed shell species. Neutral Na_4Al_{12} is a geometrically symmetrical, energetically stabilized cluster that is home to an Al_{12} moiety with a negative charge of $-3.43e$, i.e., the multiply negatively charged Zintl anion, $Al_{12}^{3.43-}$.

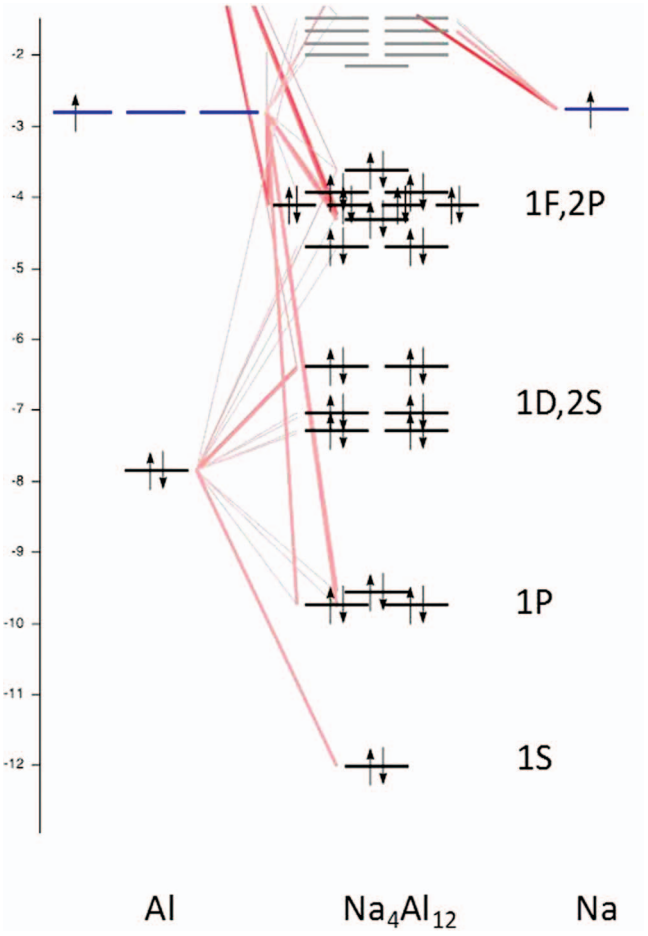

FIG. 16. The fragment molecular orbitals (FMO) analysis for the Na_4Al_{12} neutral cluster.

IV. CONCLUDING REMARKS

Through natural population (charge) analysis, we have established that the aluminum moieties within the sodium–aluminum clusters studied here are Zintl anions. Our computational results are validated by the good agreement between the values in Table I and between the computed stick spectra and their corresponding experimental photoelectron spectra. Roughly speaking, the charge on the aluminum moieties in the lowest energy isomers of both the neutral and the anionic sodium–aluminum clusters tends to be more negative for those clusters which possess larger numbers of sodium atoms. After all, sodium atoms are the primary sources of the electrons. Also, the differences between charges on the aluminum moieties in cluster anions and those on the aluminum moieties in their neutral cluster counterparts tend to be bigger, i.e., more negative, the larger the clusters' aluminum atom to sodium atom ratios. Furthermore, the charge distributions in sodium–aluminum cluster anions are consistent with those found in alkali and ammonium halide anions.[55,56] In the latter cases, the halide anionic moieties, within the larger molecular anions, carry −1e charge relative to their formally neutral alkali atom or ammonium radical partners. While the sodium moieties within sodium-aluminum cluster anions are not neutral and while their aluminum moieties carry more than one electron's worth of negative charge (they are Zintl anions),

the aluminum moieties nevertheless carry a net −1e negative charge relative to their positively charged sodium moieties, just as in the anions of simpler salts.

A salt-like lattice made up of multiply charged, aluminum cluster anions, i.e., aluminum Zintl anions, and a charge-balancing number of counter-cations might be expected to achieve high lattice stabilization (cohesion) energy and with it, the potential of forming a bulk ionic (cluster-assembled) material. Although such materials would be metastable in a thermodynamic sense, they might nevertheless be stable on a practical time scale. As bulk materials, these compositions would carry an overall charge of zero. Thus, the basic units/building blocks of these materials would need to be uncharged as well. For this reason, the characterization of aluminum Zintl anions in *neutral* sodium–aluminum clusters has been our focus in this work. The neutral sodium–aluminum clusters are simply more relevant, than are sodium–aluminum cluster anions, for making a cluster-assembled material. Moreover, neutral sodium–aluminum clusters that also exhibit closed electronic shell would make, because of their enhanced stability, particularly promising candidates as building blocks of imagined bulk materials. The neutral clusters, Na_5Al_5 and Na_4Al_{12}, not only meet this condition, but with charges of −3.67 and −3.43, respectively, their aluminum moieties exhibit the highest negative charges seen in this work. These moieties are both robust aluminum Zintl anions.

Finally, two follow-on ideas come to mind. One involves utilizing more electropositive "atoms" than alkali metal atoms with which to form clusters with aluminum "Zintl" anions. Super-alkali molecules, such as Li_3O, are candidates.[57] Another approach is to make use of sodium–aluminum cluster anions as building blocks. After all, some of them are closed shell species, and strictly speaking, their aluminum moieties are also Zintl anions. The way to do this might be to form neutral salt clusters which are made up of alkali–aluminum cluster anions and electropositive atom cations, e.g., $Cu^+(Na_mAl_n)^-$, $Mg^{++}(Na_mAl_n)^=$, or $Li^+(Cs_mAl_n)^-$.

ACKNOWLEDGMENTS

This material is based in part on work supported by the Air Force Office of Scientific Research (AFOSR) under Grant Nos. FA9550-11-1-0068 (K.H.B.) and FA9550-11-1-0171 (B.W.E.). K.H.B. and B.W.E. also thank the Defense Threat Reduction Agency (DTRA) for partial support under Grant No. HDTRA-1-12-1-007. B.K. acknowledges financial support from the BoR-RCS grant. PJ acknowledges partial support by the U. S. Department of Energy, Office of Basic Energy Sciences, Division of Materials Sciences and Engineering under Award # DE-FG02-96ER45579. Resources of the National Energy Research Scientific Computing Center supported by the Office of Science of the U.S. Department of Energy under Contract No. DE-AC02-05CH11231 is also acknowledged.

[1]F. Laves, Naturwissenschaften **29**, 244 (1941).
[2]W. Klemm and E. Busmann, Z. Anorg. Allg. Chem. **319**, 297 (1963).
[3]*Zintl Ions: Principle and Recent Developments*, edited by T. F. Fassler (Springer-Verlag, Berlin, 2011).
[4]E. Zintl and W. Dullenkopf, Z. Phys. Chem. B **16**, 183 (1932).
[5]J. D. Corbett, Chem. Rev. **85**, 383 (1985).
[6]W. Klemm, Proc. Chem. Soc. **1958**, 329 (1958).
[7]H. G. von Schnering, J. Wolf, D. Weber, R. Ramirez, and T. Meyer, Angew. Chem., Int. Ed. Engl. **25**, 353 (1986).
[8]M. Reil and N. Korber, Z. Anorg. Allg. Chem. **633**, 1599 (2007).
[9]C. Suchentrunk, J. Daniels, M. Somer, W. Carrillo-Cabrera, and N. Korber, Z. Naturforsch. B **60**, 277 (2005).
[10]A. Spiekermann, S. D. Hoffmann, and T. F. Fassler, Angew. Chem., Int. Ed. Engl. **45**, 3459 (2006).
[11]V. Queneau, E. Todorov, and S. C. Sevov, J. Am. Chem. Soc. **120**, 3263 (1998).
[12]S. Joseph, C. Suchentrunk, F. Kraus, and N. Korber, Eur. J. Inorg. Chem. **2009**, 4641 (2009).
[13]R. W. Farley and A. W. Castleman, J. Am. Chem. Soc. **111**, 2734 (1989).
[14]R. W. Farley and A. W. Castleman, J. Chem. Phys. **92**, 1790 (1990).
[15]W. J. Zheng, O. C. Thomas, J. M. Nilles, K. H. Bowen, A. C. Reber, and S. N. Khanna, J. Chem. Phys. **134**, 224307 (2011).
[16]A. E. Kuznetsov, A. I. Boldyrev, X. Li, and L. S. Wang, J. Am. Chem. Soc. **123**, 8825 (2001).
[17]L. F. Cui, X. Huang, L. M. Wang, D. Y. Zubarev, A. I. Boldyrev, J. Li, and L. S. Wang, J. Am. Chem. Soc. **128**, 8390 (2006).
[18]L. F. Cui, X. Huang, L. M. Wang, J. Li, and L. S. Wang, J. Phys. Chem. A **110**, 10169 (2006).
[19]J.-P. Dognon, C. Clabaguera, and P. Pyykko, Angew. Chem., Int. Ed. **46**, 1427 (2007).
[20]A. Grubisic, H. Wang, X. Li, Y.-J. Ko, F. S. Kocak, M. R. Pederson, K. H. Bowen, and B. W. Eichhorn, Proc. Natl. Acad. Sci. U.S.A. **108**, 14757 (2011).
[21]L.-F. Cui, X. Huang, L.-M. Wang, J. Li, and L. S. Wang, Angew. Chem., Int. Ed. **46**, 742 (2007).
[22]U. Rohrmann, S. Schaefer, and R. Schaefer, J. Phys. Chem. A **113**, 12115 (2009).
[23]D. E. Ellis, G. A. Benesh, and E. Byrom, Phys. Rev. B **16**, 3308 (1977).
[24]A. Zunger, Phys. Rev. B **17**, 2582 (1978).
[25]K. Kishio and J. O. Brittain, J. Phys. Chem. Solids **40**, 933 (1979).
[26]N. E. Christensen, Phys. Rev. B **32**, 207 (1985).
[27]R. Nesper, Angew. Chem., Int. Ed. Engl. **30**, 789 (1991).
[28]A. Purath, R. Koppe, and H. Schnoeckel, Angew. Chem., Int. Ed. **38**, 2926 (1999).
[29]P. Henke, N. Trapp, C. E. Anson, and H. Schnoeckel, Angew. Chem., Int. Ed. **49**, 3146 (2010).
[30]R. E. Leuchtner, A. C. Harms, and A. W. Castleman, J. Chem. Phys. **94**, 1093 (1991).
[31]X. Li, H. Wu, X.-B. Wang, and L. S. Wang, Phys. Rev. Lett. **81**, 1909 (1998).
[32]S. N. Khanna and P. Jena, Phys. Rev. B **51**, 13705 (1995).
[33]F. Liu, M. Mostoller, T. Kaplan, S. N. Khanna, and P. Jena, Chem. Phys. Lett. **248**, 213 (1996).
[34]S. N. Khanna, B. K. Rao, and P. Jena, Phys. Rev. B **65**, 125105 (2002).
[35]A. Nakajima, K. Hoshino, T. Sugioka, T. Naganuma, T. Taguwa, Y. Yamada, K. Watanabe, and K. Kaya, J. Phys. Chem. **97**, 86 (1993).
[36]K. Hoshino, K. Watanabe, Y. Konishi, T. Taguwa, A. Nakajima, and K. Kaya, Chem. Phys. Lett. **231**, 499 (1994).
[37]W.-J. Zheng, O. C. Thomas, T. P. Lippa, S. J. Xu, and K. H. Bowen, J. Chem. Phys. **124**, 144304 (2006).
[38]Y. J. Ko, A. Shakya, H. Wang, A. Grubisic, W. Zheng, M. Goetz, G. Gantefoer, K. H. Bowen, P. Jena, and B. Kiran, J. Chem. Phys. **133**, 124308 (2010).
[39]O. C. Thomas, W.-J. Zheng, T. P. Lippa, S. J. Xu, and K. H. Bowen, J. Chem. Phys. **114**, 9895 (2001).
[40]O. C. Thomas, W.-J. Zheng, and K. H. Bowen, J. Chem. Phys. **114**, 5514 (2001).
[41]X. Li, A. E. Kuznetsov, H.-F. Zhang, A. I. Boldyrev, and L. S. Wang, Science **291**, 859 (2001).
[42]A. E. Kuznetsov, A. I. Boldyrev, H. J. Zhai, X. Li, and L. S. Wang, J. Am. Chem. Soc. **124**, 11791 (2002).
[43]A. E. Kuznetsov, K. A. Birch, A. I. Boldyrev, X. Li, H. J. Zhai, and L. S. Wang, Science **300**, 622 (2003).
[44]A. Dhavale, D. G. Kanhere, S. A. Blundell, and R. R. Zope, Phys. Rev. B **65**, 085402 (2002).
[45]N. Walsh, F. Martinez, G. Marx, and L. Schweikhard, Eur. Phys. J. D **43**, 241 (2007).

[46]W. D. Knight, K. Clemenger, W. A. de Heer, W. A. Saunders, M. Y. Chou, and M. L. Cohen, Phys. Rev. Lett. **52**, 2141 (1984).
[47]F. M. Bickelhaupt and E. J. Baerends, in *Reviews in Computational Chemistry*, edited by K. B. Lipowitz and D. B. Boyd (Wiley, New York, 2000), Vol. 15, pp. 1–86.
[48]M. Gerhards, O. C. Thomas, J. M. Nilles, W. J. Zheng, and K. H. Bowen, J. Chem. Phys. **116**, 10247 (2002).
[49]X. Li, A. Grubisic, S. T. Stokes, J. Cordes, G. F. Gantefoer, K. H. Bowen, B. Kiran, M. Willis, P. Jena, R. Burgert, and H. Schnoeckel, Science **315**, 356 (2007).
[50]J. Ho, K. M. Ervin, and W. C. Lineberger, J. Chem. Phys. **93**, 6987 (1990).
[51]M. J. Frisch, G. W. Trucks, H. B. Schlegel *et al.*, GAUSSIAN 03, Revision C.02, Gaussian, Inc., Wallingford, CT, 2004.
[52]G. te Velde, F. M. Bickelhaupt, S. J. A. van Gisbergen, C. Fonseca Guerra, E. J. Baerends, J. G. Snijders, and T. Ziegler, J. Comput. Chem. **22**, 931 (2001).
[53]C. Fonseca Guerra, J. G. Snijders, G. te Velde, and E. J. Baerends, Theor. Chem. Acc. **99**, 391 (1998).
[54]ADF2013, SCM, Theoretical Chemistry, Vrije Universiteit, Amsterdam, The Netherlands, http://www.scm.com.
[55]T. M. Miller, D. G. Leopold, K. K. Murray, and W. C. Lineberger, J. Chem. Phys. **85**, 2368 (1986).
[56]S. N. Eustis, D. Radisic, K. H. Bowen, R. A. Bachorz, M. Haranczyk, G. K. Schenter, and M. Gutowski, Science **319**, 936 (2008).
[57]D. Wang, J. D. Graham, A. M. Buytendyk, and K. H. Bowen, J. Chem. Phys. **135**, 164308 (2011).

DOI: 10.1002/zaac.201300359

K[$Al_4(PPh_2)_7PPh$]: An Al^{II} Phosphanide / Phosphinidene Intermediate on the Path to AlP Formation

Dennis H. Mayo,[a,b] Yang Peng,[a] Samantha DeCarlo,[a] Xiang Li,[c] James Lightstone,[b] Peter Zavalij,[a] Kit Bowen,[c] Hansgeorg Schnöckel,[d] and Bryan Eichhorn*[a]

Dedicated to Professor Werner Uhl on the Occasion of His 60th Birthday

Keywords: Aluminum; Phosphanide; Phospinidene

Abstract. The reaction of metastable $AlCl{\cdot}(Et_2O)_n$ with potassium diphenylphosphanide results in the formation of the aluminum(II) phosphanide / phosphinidene K[$Al_4(PPh_2)_7PPh$] compound, which is the first reported aluminum(II) phosphinidene complex. The Al^{II} structure results from ligand decomposition and represents the first step in the conversion of $AlPPh_2$ to AlP and biphenyl.

Introduction

Low oxidation state aluminum compounds have drawn considerable interest due to their unprecedented structural chemistry,[1] unusual chemical reactivity[2–4] and their propensity for metal-metal bond formation.[5–7] Solutions of Al^{I} halides have proven to be excellent precursors to low oxidation state Al^{I} complexes,[7] such as $Al_4Cp^*_4$,[8] but can also undergo redox (disproportionation) reactions to give new classes of clusters and compounds containing Al oxidation states from 0.27 to 3.0.[1,7] The most famous of these are the Al metalloid clusters that can be isolated during the disproportionation process: $3Al^{1+} \rightarrow Al^{3+} + 2\ Al^0$. These clusters, such as $[Al_{77}\{N(SiMe_3)_2\}_{20}]^{2-}$, can be trapped due to the presence of various kinetic barriers on the way to forming aluminum metal and represent the transition from large metallic clusters to small metallic nanoparticles. Recently, we have shown that a completely different reaction pathway is viable with some ligand systems in which ligand redox chemistry can lead to salt-like aluminum binaries. In particular, dialkyl phosphanides (R_2P^- where R = *t*Bu), react with Al^{I} halides to give $Al_2(PR_2)_4$, $Al_4(PR_2)_6$, $Al_8Br_8(PR_2)_6$ and the intriguing $Al_3P(PR_2)_4Cl_2$.[9–11] The latter complex contains a naked P^{3-} ion that presumably results from a successive ligand-based decomposition process leading to the Al_3P moiety. DFT studies showed how the ligand redox vs. disproportionation pathways followed different routes from the Al^{I} precursors to give markedly different products.[10] The propensity of the phosphanide ligands to bridge between two aluminum atoms seems to preclude the formation of metalloid clusters and propels the system into the ligand based redox pathway. We describe here a fortuitous isolation of an intermediate along this pathway that provides additional evidence for the ligand-based decomposition process. The intermediate complex, K[$Al_4(PPh_2)_7PPh$], is formed during the reaction of $AlCl{\cdot}(Et_2O)_n$ with potassium diphenylphosphanide and contains Al^{II} ions and a PhP^{2-} phosphinidene ligand in addition to the expected phosphanide ligands,. The isolation and characterization of this complex represents the first step in the formation of AlP from phosphanide precursors.

* Prof. Dr. B. Eichhorn
E-Mail: eichhorn@umd.edu
[a] Department of Chemistry and Biochemistry
University of Maryland, College Park
College Park, MD 20742, USA
[b] Research Department
Indian Head EOD Technology Division
Naval Surface Warfare Center
Indian Head, MD 20640, USA
[c] Departments of Chemistry and Materials Science
Johns Hopkins University
Baltimore, MD 21218, USA
[d] Institute of Inorganic Chemistry
and Center for Functional Nanostructures (CFN)
Karlsruhe Institute of Technology
76128 Karlsruhe, Germany
Supporting information for this article is available on the WWW under http://dx.doi.org/10.1002/zaac.201300359 or from the author.

Results and Discussion

The title complex was prepared from the reaction of a cold (–78 °C) solution of $AlCl{\cdot}(Et_2O)_n$ with a solution of potassium diphenylphosphanide in diethyl ether. This reaction mixture was warmed to room temperature overnight, evaporated to dryness and extracted into toluene. Storage of the reaction mixture at –25 °C for six months resulted in the formation of a few yellow crystals of K[$Al_4(PPh_2)_7PPh$]·$HPPh_2$·4 C_7H_8 (**1**) on the vessel wall. For **1**, the inclusion of the non-coordinated phosphane solvate ($HPPh_2$) in the crystal lattice suggests incomplete deprotonation of $HPPh_2$ in the production of the $KPPh_2$ precursor used in the reaction.

Zeitschrift für anorganische und allgemeine Chemie ZAAC Journal of Inorganic and General Chemistry

The ESI-MS studies of the reaction mixtures showed the presence of the closely related $[Al_4(PPh_2)_6(PPh)_2KCl]^-$, $[Al_5(PPh_2)_7HKCl]^-$ and $[Al_5(PPh_2)_6HKCl]^-$ clusters in solution (Figure S3) but **1** was not observed; presumably due to its insolubility.

The solid-state X-ray crystal structure of **1** contains polymeric chains of $[Al_4(PPh_2)_7PPh]^-$ units (Figure 1 and Figure S1). Each $[Al_4(PPh_2)_7PPh]^-$ unit contains two Al–Al pairs, three bridging diphenylphosphanide ligands, four terminal diphenylphosphanide ligands, and one terminal phenylphosphinidene ligand. The idealized $(AlP)_4P_4$ core comprises four fused cyclopentane-like rings with a bis-noradamantane structure[12] and has virtual D_{2d} point symmetry (Figure 1). The ring structure is reminiscent of the P_4Al_6 adamantane-like core in $P_4(AlCp^*)_6$ and the Ga_4P_{10} core in $Ga_{16}(PtBu_2)_{10}$ that contains an inverse P_4O_{10} structure.[13,14] However, when the asymmetry of the lone phosphinidene ligand is considered, the $(AlP)_4P_4$ core has virtual C_2 symmetry with a C_2 axis of rotation passing through P1 and P5. The aluminum atoms are formally +2 and each achieves an 8-electron configuration through Al–P coordinate bonds and Al–Al interactions. The terminal phosphorus atoms are all distinctly pyramidalized as evidenced by the 106 +/– 5 °C–P–C bond angles. Trigonal pyramidal geometries for the terminal phosphanide ligands are indicative of non-interacting lone pairs on phosphorus, consistent with aluminum atoms that are electronically saturated from the σ-bonding framework.

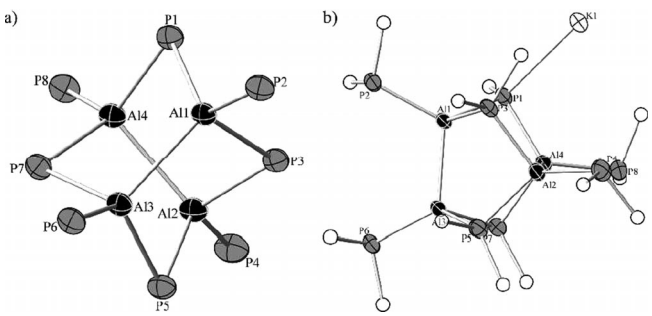

Figure 1. X-ray crystal structure of 1 a) without and b) with the potassium atom. Thermal ellipsoids drawn at the 50% probability level, hydrogen and carbon atoms omitted for clarity. The phosphinidine ligand contains the phosphorus atom P1. Selected bond lengths /Å and angles /°: Al1–Al3 2.643(2), Al2–Al4 2.655(2), Al1–P1 2.380(1), Al1–P2 2.428(2), Al1–P3 2.450(2), Al2–P3: 2.429(2), Al2–P4 2.402(2), Al2–P5 2.457(1), Al3–P5 2.436(1), Al3–P6 2.392(1), Al3–P7 2.424(1), Al4–P7 2.436(1), Al4–P8 2.395(2), Al4–P1 2.365(1), P1–K1 3.182(1), Al1–P1–Al4 91.12(5), Al2–P5–Al3 93.62(5).

The Al–Al bond lengths in **1,** 2.642(2) and 2.655(21) Å, are similar to those of other aluminum(II) compounds containing Al–Al bonds. For example, the Al–Al bond lengths in [{(IPr)$(H)_2Al\}_2$] (IPr =C{$(DipNCH)_2$}, Dip = 2,6-diisopropylphenyl) and Al_2Br_4·2 anisole are 2.638(1) and 2.527(1) Å, respectively.[6,15] The four non-bonding Al···Al separations in **1** are in the range 3.385(1) to 3.581(1) Å.

The Al–P bond lengths involving the terminal and bridging phosphanide ligands are in the ranges 2.425(8) to 2.459(8) [2.445(3) Å, av.], and 2.392(5) to 2.421(3) [2.412(4) Å, av.], respectively. The distances are quite similar to those in Al^{III} phosphanide complexes[16] and other low oxidation state Al–P complexes (i.e. Al–P bonds ranging from 2.308 to 2.422 Å in $[P_4(AlCp^*)_6]$.[13] The phosphorus atom of the phosphinidene ligand (P1) is tetracoordinate, with one P–C bond (1.767(1) Å), one P–K bond (3.182(1) Å), and two P–Al bonds (2.379(1) and 2.365(1) Å). The latter are slightly shorter than the average P–Al bonds of the phosphanide ligands in **1**, and longer than the Al–P bond lengths in the Al^{III} phosphinidine reported by *Power* (average Al–P 2.328(3) Å).[17] The small distortion in phosphinidine Al–P bond lengths imparts a more acute Al1–P1–Al4 bond angle of 91.12(5)° relative to the others (Al–P–Al = 94.3°, av.) and results in a non-bonding Al1–Al4 distance of 3.387(2) Å. This separation is shorter than the others (3.577(3) Å, av.) and slightly distorts the Al_4P_8 core from the idealized bis-noradamantane structure.

The phosphinidine ligand forms a coordinate bond to the potassium ion, which is in turn intramolecularly bound to two phenyl rings through η^6-interactions from two diphenylphosphanide moieties within the $[Al_4(PPh_2)_7PPh]^-$ unit (Figure 2). The phenyl ring of the P6 diphenylphosphanide ligand in a neighboring $[Al_4(PPh_2)_7PPh]^-$ unit is also coordinated to the K^+ ion in an η^6-fashion. The potassium ion has nineteen total bonding contacts in a 1+6+6+6 coordination pattern, with K–C bonding distances in the range of 3.018(4) to 3.424(4) Å (Figure 2). The chain can be viewed as a series of $[Al_4(PPh_2)_7PPh]^-$ units held together by a K–P coordinate bond and cation–π interactions between the potassium ion and phenyl rings (Figure S2a). Similar alkali metal–π interactions are known in organometallic polymers prepared in arene solvents[18] as well as sodium-containing 'dialuminyne' species.[5] The $[Al_4(PPh_2)_7PPh]^-$ units are chiral and form homochiral chains that propagate along the 2_1 screw axis of the crystal lattice. Chains of alternating chirality pack in layers separated by the layers of solvate molecules (Figure S2b).

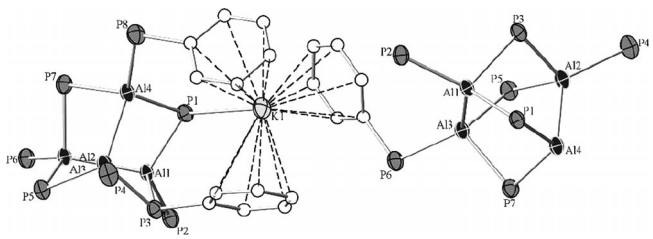

Figure 2. Drawing of the potassium ion coordination sphere in **1**. Carbon atoms (white) are isotropic whereas the K (light gray) and P (gray) atom thermal ellipsoids are drawn at the 50% probability level. Select atoms omitted for clarity. Average K–C(centroid) distance 2.925 Å.

Conclusions

The Al/P core of complex **1** is closely related to the previously-reported aluminum phosphanide clusters $Al_2(PR_2)_4$ (2) and $Al_4(PR_2)_6$ (3) where R = *t*Bu.[9,11] Although the alkyl substituent of the phosphanides differs, the Al/P frameworks in all three compounds have notably similarities in Al–P coordination and metric parameters. These structures are shown in the SI.

The disproportionation reactions involving AlX precursors to give low oxidation state metalloids and other oxidized aluminum cluster compounds require ligand scrambling and multiple electron transfers. While the mechanistic details of formation are always difficult to discern, the products give clues about general reaction pathways. The formation of the phosphinidene ligand presumably results from a redox reaction of a coordinated Al–PPh_2, which is the first step on the pathway to AlP formation that can simplistically be viewed as: $Al(PPh_2) \rightarrow AlP + Ph_2$. The prior isolation of the Al_3P complex $PAl_3(PR_2)_4Cl_2$ (R = *t*-Bu) represents a subsequent step in oxidative decomposition of aluminum phosphanide complexes to give the thermodynamic end product AlP.[10] In contrast, disproportionation of a metastable "$GaPR_2$" solution (formed during the reaction of GaX with $LiPR_2$) is favored, resulting in metalloid clusters such as $Ga_{16}(GaPR_2)_{10}$[14] and $Ga_{51}(PR_2)_{14}Br_6$.[19] These clusters contain cores of "naked" gallium atoms, such as a Ga_4 unit in the Ga_{16} cluster and a cuboctahedral Ga_{13} unit in the Ga_{51} cluster, which are surrounded by bridging and terminal $GaPR_2$ moieties.[14,19] These clusters have been discussed to be precursors for core-shell nanoparticles containing a metallic gallium core and a semiconducting GaP shell.[19] Therefore, the formation of **1** in small quantities may be a hint that the main product may be an intermediate metalloid $Al_n(AlPR_2)_m$ ($n>m$) cluster on the way to an AlP particle, which is similar to the GaP shells described above.

Experimental Section

General Considerations: All reactions are performed under a dinitrogen atmosphere in a glovebox or under argon using standard Schlenk techniques. Toluene and diethyl ether were purified by distillation from sodium benzophenone ketyl under a dinitrogen atmosphere. All purified solvents were stored in modified Schlenk vessels over 3 Å molecular sieves under a dinitrogen atmosphere. Diphenylphosphane was purchased as a 10% (w/w) solution in hexane from Strem and the hexane was removed in vacuo immediately prior to use.

$AlCl{\cdot}(Et_2O)_n$: Aluminum metal (0.950 g, 35.2 mmol) was reacted with gaseous HCl (36.5 mmol) over 3 h at approx. 1200 K in a modified *Schnöckel*-type metal halide co-condensation reactor.[20,21] The resultant gas-phase AlCl was co-condensed with a mixture of toluene:diethyl ether (4:1 v/v) at approx. 77 K. The solvent matrix was thawed to –80 °C and the resultant yellow-brown solution stored at that temperature prior to use.[20,21] Titration of the $AlCl{\cdot}(Et_2O)_n$ solution via Mohr's method determined a chloride concentration of 220 mM and an Al:Cl ratio of 1:1.03.

$K[Al_4(PPh_2)_7PPh]_n$ (1): Diphenylphosphane (500 mg, 2.68 mmol) was dissolved in diethyl ether (75 mL) and this solution added dropwise via cannula onto potassium metal (117 mg, 3.0 mmol) at room temperature. The resulting orange reaction mixture was stirred vigorously for 20 h, filtered via cannula, and concentrated to approximately 5 mL in vacuo. The reaction mixture was then cooled to –78 °C and $AlCl{\cdot}(Et_2O)_n$ (2.55 mmol, 11.6 mL of a 220 mM solution in toluene:diethyl ether 4:1) was added via syringe. The brown reaction mixture was warmed from –78 °C to room temperature over 2 h and stirred at for 16 h. The resulting dark brown reaction mixture was evaporated to dryness in vacuo and extracted into toluene (approx. 25 mL). The brown solution was filtered via cannula, further concentrated to approx. 5 mL, and heated at 65 °C for 4 days. The reaction mixture was then placed in a –15 °C freezer, where a few small yellow crystals of **1** suitable for single crystal x-ray analysis formed on the glass wall after six months. X-ray crystal data: Bruker APEX-II CCD (Mo-K_α sealed tube, λ = 0.71073 Å); final *R* indices (all data): R_1 = 0.0663, ωR_2 = 0.1097.

Supporting Information (see footnote on the first page of this article)**:** Additional drawings of the molecular structure and crystallographic data and ESI-MS data. See CCDC reference number 934411 for crystallographic .cif file.

Acknowledgments

This work was supported by AFSOR (Program manager M. Berman), DTRA (Program managers S. Peiris, W. Wilson), and the National Science Foundation (BWE), the ASEE SMART Program (DHM), the Deutsche Forschungsgemeinschaft (HS), and the Air Force Office of Scientific Research under grant no. FA9550–11–1-0068 (KHB).

References

[1] A. Ecker, E. Weckert, H. Schnöckel, *Nature* **1997**, *387*, 379–381.
[2] H. Schnöckel, M. Leimkühler, R. Lotz, R. Mattes, *Angew. Chem. Int. Ed. Engl.* **1986**, *25*, 921–922.
[3] C. Dohmeier, R. Mattes, H. Schnöckel, *J. Chem. Soc., Dalton Trans.* **1990**, 358–359.
[4] Y. Zhao, Y. Liu, Y. Lei, B. Wu, X.-J. Yang, *Chem. Commun.* **2013**, *49*, 4546–4548.
[5] R. J. Wright, M. Brynda, P. P. Power, *Angew. Chem. Int. Ed.* **2006**, *45*, 5953–5956.
[6] S. J. Bonyhady, D. Collis, G. Frenking, N. Holzmann, C. Jones, A. Stasch, *Nature Chem.* **2010**, *2*, 865–869.
[7] H. Schnöckel, *Chem. Rev.* **2010**, *110*, 4125–4163.
[8] C. Dohmeier, C. Robl, M. Tacke, H. Schnöckel, *Angew. Chem. Int. Ed. Engl.* **1991**, *30*, 564–565.
[9] P. Henke, M. Huber, J. Steiner, K. H. Bowen, B. W. Eichhorn, H. Schnöckel, *J. Am. Chem. Soc.* **2009**, *131*, 5698–5704.
[10] P. Henke, H. Schnöckel, *Chem. Eur. J.* **2009**, *15*, 13391–13398.
[11] P. Henke, T. Pankewitz, W. Klopper, F. Breher, H. Schnöckel, *Angew. Chem. Int. Ed.* **2009**, *48*, 8141–8145.
[12] B. R. Vogt, S. R. Suter, J. R. E. Hoover, *Tetrahedron Lett.* **1968**, *9*, 1609–1612.
[13] C. Dohmeier, H. Schnöckel, C. Robl, U. Schneider, R. Ahlrichs, *Angew. Chem. Int. Ed. Engl.* **1994**, *33*, 199–200.
[14] J. Steiner, G. Stösser, H. Schnöckel, *Angew. Chem. Int. Ed.* **2003**, *42*, 1971–1974.
[15] M. Mocker, C. Robl, H. Schnöckel, *Angew. Chem. Int. Ed. Engl.* **1994**, *33*, 862–863.
[16] J. F. Janik, E. N. Duesler, W. F. McNamara, M. Westerhausen, R. T. Paine, *Organometallics* **1989**, *8*, 506–514.
[17] R. J. Wehmschulte, P. P. Power, *J. Am. Chem. Soc.* **1996**, *118*, 791–797.
[18] J. J. Morris, B. C. Noll, G. W. Honeyman, C. T. O'Hara, A. R. Kennedy, R. E. Mulvey, K. W. Henderson, *Chem. Eur. J.* **2007**, *13*, 4418–4432.
[19] J. Steiner, G. Stösser, H. Schnöckel, *Angew. Chem. Int. Ed.* **2004**, *43*, 302–305.
[20] P. Timms, *Acc. Chem. Res.* **1973**, *6*, 118–123.
[21] M. Tacke, H. Schnöckel, *Inorg. Chem.* **1989**, *28*, 2895–2896.

Received: July 19, 2013
Published Online: October 30, 2013

Dedicated Cluster

DEPARTMENT OF DEFENSE

DEFENSE THREAT REDUCTION
AGENCY
8725 JOHN J. KINGMAN ROAD
STOP 6201
FORT BELVOIR, VA 22060
ATTN: A. DALTON

DEFENSE TECHNICAL
INFORMATION CENTER
8725 JOHN J. KINGMAN ROAD,
SUITE 0944
FT. BELVOIR, VA 22060-6201
ATTN: DTIC/OCA

DEPARTMENT OF DEFENSE CONTRACTORS

QUANTERION SOLUTIONS, INC.
1680 TEXAS STREET, SE
KIRTLAND AFB, NM 87117-5669
ATTN: DTRIAC